Nanotoxicology, August 2014; 8(5):485–507

ISSN: 1743-5390 print / 1743-5404 online
DOI: 10.3109/17435390.2013.801089

informa
healthcare

Neoplastic-like transformation effect of single-walled and multi-walled carbon nanotubes compared to asbestos on human lung small airway epithelial cells

Liying Wang[1,*], Todd A. Stueckle[1,2,*], Anurag Mishra[1], Raymond Derk[1], Terence Meighan[1], Vincent Castranova[1], & Yon Rojanasakul[2]

[1]*HELD/PPRB, National Institute for Occupational Safety and Health, Morgantown, WV 26505, USA and* [2]*School of Pharmacy, West Virginia University, Morgantown, WV 26506, USA*

Abstract

Accumulating evidence indicates that carbon nanotubes (CNTs) are biopersistent and can cause lung damage. With similar fibrous morphology and mode of exposure to asbestos, a known human carcinogen, growing concern has arisen for elevated risk of CNT-induced lung carcinogenesis; however, relatively little is known about the long-term carcinogenic effect of CNT. Neoplastic transformation is a key early event leading to carcinogenesis. We studied the ability of single- and multi-walled CNTs to induce neoplastic transformation of human lung epithelial cells compared to asbestos. Long-term (6-month) exposure of the cells to occupationally relevant concentrations of CNT in culture caused a neoplastic-like transformation phenotype as demonstrated by increased cell proliferation, anchorage-independent growth, invasion and angiogenesis. Whole-genome expression signature and protein expression analyses showed that single- and multi-walled CNTs shared similar signaling signatures which were distinct from asbestos. These results provide novel toxicogenomic information and suggest distinct particle-associated mechanisms of neoplasia promotion induced by CNTs and asbestos.

Keywords: lung, neoplastic transformation, invasion, genome expression, microarray

Introduction

Engineered nanomaterials (ENMs), including carbon nanotubes (CNTs), have recently emerged as one of the most important classes of nanomaterials having enormous potential to initiate the next industrial revolution. According to the National Science Foundation, it is estimated that by 2020 nanotechnology will have a $3 trillion impact on the global economy and employ 6 million workers in the manufacture of nanomaterial-based products, 2 million of which may be in the United States. CNTs, including single-walled CNT (SWCNT) and multi-walled CNT (MWCNT), are widely used in nanotechnology (Roco 2005; Shvedova et al. 2005; Hussain et al. 2009). Their unique characteristics provide many benefits to a wide number of applications and their use is expected to rapidly grow in industrial and consumer products (Donaldson et al. 2010). However, properties of CNT, such as high aspect ratio (HAR), bio-persistence and reactive oxygen species (ROS) generation ability, have raised concern of asbestos-like adverse effects to human health (Roco 2005; Shvedova et al. 2005; Hussain et al. 2009; Donaldson et al. 2010; Murphy et al. 2011). With a HAR, SWCNT and MWCNT typically exhibit fibre-like characteristics similar to asbestos, a Group I human carcinogen designated by the International Agency of Research in Cancer (Roco 2005; Shvedova et al. 2005, Donaldson et al. 2010; Hussain et al. 2009). Given known workplace exposure, anticipated widespread use and asbestos-like fibre similarities, it is critical that investigations study expected CNT exposure scenarios to adequately assess CNT occupational and environmental risk to long-term human health (Aschberger et al. 2010; Donaldson et al. 2010).

The lung is the major target organ for airborne ENM exposures. *In vivo* studies show nano-scaled SWCNT and MWCNT reaching deep tissue layers of the lung with low clearance. Persistence of inhaled ENMs associated with lung cells can last at least 2 months (Muller et al. 2005), while ~90% w/w inhaled MWCNT that penetrate lung tissue can persist in mouse lung 6 months post-exposure (Mercer et al. 2012). Persistent retention of HAR particles, including CNTs, result in chronic interaction with lung tissues and cells such as small airway epithelial cells (SAECs; Donaldson et al. 2010; Mercer et al. 2010; Broaddus et al. 2011). Such findings have given rise to immediate concern that chronic interactions of these persistent HAR nanoparticles with lung cells could potentially pose an elevated risk for inducing or promoting carcinogenesis.

Correspondence: Liying Wang, HELD/PPRB, National Institute for Occupational Safety and Health, 1095 Willowdale Road, Morgantown WV 26505, USA. Tel: +1 304 285 6349 opt. 1 & 3. E-mail: lmw6@cdc.gov and jux5@cdc.gov
*Both authors contributed equally to this work.

(Received 15 October 2012; accepted 28 April 2013)

Asbestos has been long known to cause pulmonary fibrosis, lung cancer and malignant mesothelioma which have been linked to its fibrous shape, Fe ion residues, increased ROS production, mutagenicity and chronic inflammation (Kamp 2009; Broaddus et al. 2011). Single dose and recent subchronic murine inhalation studies have shown that CNT and asbestos can deposit at the bronchial alveolar duct junction and penetrate interstitially with a small significant fraction making it to the pleural cavity (Yin et al. 2007; Mercer et al. 2008; Mercer et al. 2011). CNT deposition in the lung results in ROS generation, inflammation, macrophage recruitment, immune suppression, granulomas and interstitial fibrosis, similar to asbestos (Lam et al. 2004; Muller et al. 2005; Shvedova et al. 2005; Mitchell et al. 2009; Shvedova et al. 2009; Murray et al. 2012). CNT injected into the abdominal cavity of mice at high concentrations resulted in increased inflammation and mesothelioma development similar to asbestos (Poland et al. 2008; Takagi et al. 2008; Nagai et al. 2011). A recent preliminary study suggested that MWCNT inhalation exposure promotes lung carcinogenesis in a murine initiation/promotion tumour model (Sargent et al. 2013). At present, no published *in vivo* studies exist providing conclusive evidence that chronic inhalation of CNT at occupationally relevant doses poses a risk for lung carcinogenesis. Even though CNTs exhibit asbestos-like qualities, several CNT exposure studies reported potentially different lung burden transport mechanisms (Mercer et al. 2010), transient inflammation and rapid onset of fibrosis (Shvedova et al. 2005; Mercer et al. 2008; Porter et al. 2010) which conflicts with the hypothesised mechanism for asbestos-related lung disease. It is possible that given the unique physicochemical properties of CNT, mechanism(s) for lung disease may differ from asbestos and other known fibres (Shvedova et al. 2005; Aschberger et al. 2010; Donaldson et al. 2010; Teeguarden et al. 2011). In addition, recent work has reported that differences in CNT length, diameter, dispersion status and functionalisation impact fate, cellular uptake, persistence and response in murine lung models (Mercer et al. 2008; Mercer et al. 2011; Nagai et al. 2011; Wang et al. 2011a). Identification of physicochemical properties of fibrous nanomaterials that elicit long-term adverse outcomes is critical to further development of safe CNT technology.

Increased need to rapidly screen numerous suspected organic and metallic compounds for their ability to induce or promote carcinogenesis has resulted in development and validation of subchronic *in vitro* exposure models for neoplastic transformation (OECD 2007; Creton et al. 2012). *In vitro* neoplastic transformation can indicate a xenobiotic's potential for inducing or promoting carcinogenesis which is a complex and multistep process. Syrian hamster embryo and Balb/c 3T3 murine cell lines were recently prevalidated for cell transformation assays (Vanparys et al. 2011) while validation of a human cell model is currently lacking (Creton et al. 2012). Cells undergoing neoplastic transformation typically exhibit hallmarks such as altered morphology (i.e. block to cell differentiation), immortality via genetic instability, enhanced cancer hallmark cell behaviour and *in vivo* tumour formation (Hanahan & Weinberg 2011; Creton et al. 2012). Given projected development of new nanomaterial technologies and increased concerns with risks to human health, *in vitro* screening methods with human cell lines can provide rapid, robust and high-throughput assessments for neoplastic transformation potential of nanomaterials.

Recent *in vitro* investigations have begun to determine lung cell signalling mechanisms regulating responses to acute CNT exposures in an attempt to link them to fibrosis and lung disease; however, few chronic studies have been performed. Our previous study showed that *in vitro* chronic SWCNT exposure induced malignant transformation of human bronchial epithelial cells (BEAS-2B) associated with altered p53 signalling (Wang et al. 2011b). Acute *in vitro* studies compared different physicochemical properties of CNT to asbestos in both lung epithelial and fibroblasts. These studies report altered apoptosis, DNA damage, inflammation, morphogenesis and activation of number of signalling pathways, all of which recapitulate key molecular events involved in asbestos-induced mesothelioma (Sharma et al. 2007; Chou et al. 2008; Pacurari et al. 2008a; Pacurari et al. 2008b; Lindberg et al. 2009; Hirano et al. 2010; Kim et al. 2012; Ponti et al. 2012; Sargent et al. 2012). At present, there is a lack of understanding about genome-wide alterations in lung epithelial cell signalling mechanisms in response to chronic CNT exposure and whether these signalling mechanisms elicit an unstable genome and potential tumourigenesis.

There is an inherent lack of information on CNT-induced transformation of cultured human lung epithelial cell compared to asbestos and spherical-shaped carbon black which exhibits a minimal cytotoxic effect compared to SWCNT at equivalent mass per area dose (Wang et al. 2010). To our knowledge, only two previous studies have evaluated the cellular response to chronic exposures to CNT at realistic doses compared to asbestos, a well-known lung carcinogen (Thurnherr et al. 2011; Wang et al. 2011b). Such chronic studies are urgently needed given increased use of nanomaterials in consumer products, elevated lung disease risk observed in *in vivo* studies, and the inherent lack of mechanistic understanding of CNT-induced disease (Aschberger et al. 2010; Donaldson et al. 2010; Broaddus et al. 2011).

To address this concern, the present study employed subchronic, environmentally relevant exposures of non-tumourigenic human SAECs to dispersed SWCNT, MWCNT, asbestos or ultra-fine carbon black (UFCB) to evaluate and compare neoplastic transformation potential of these particles *in vitro*. Based on recent reports and each particle's specific morphological characteristics, we hypothesised that subchronic exposure to SAEC at an occupationally relevant dose of dispersed CNT would result in neoplastic transformation via different signalling mechanisms than what are proposed for asbestos. To test this hypothesis, post-exposure cell behaviours and whole-genome expression profiling coupled with current scientific knowledge database analysis were performed to identify novel mechanisms driving neoplastic transformation (Ganter & Giroux 2008). To date, only one study compared acute toxicogenomic signatures of human bronchial cells exposed to MWCNT to that of

Table I. Physicochemical properties of particles chronically exposed to human SAECs.

Particle	UFCB	SWCNT	MWCNT	Crocidolite asbestos
Manufacturer/Source	Cabot (Edison, NJ, USA)	CNI, Houston, TX, USA	Mitsui & Company	NIEHS, Kalahari desert
Catalog Reference	Elftex 12 (furnace black)		MWNT-7, Lot 05072001K28	CAS 12001-28-4
Synthesis	Vapour-phase pyrolysis	HiPCO	Chemical vapor deposition	Natural
Dry mean length (μm)	n/a	1–4	8.19 ± 1.7	10
Dry mean width (nm)	37	1–4	81 ± 5	210
BET surface area (m^2/g)*	43	400–1040	26	9.8
Dispersed mean length (μm)	0.93	1.08	5.1	10
Dispersed mean width (nm)	700	270	78	210
% carbon (w/w)	>99	99	99	<1
% Metal impurities (w/w)	<1	<1	0.78	50.9 for SiO_2, 38.00 for other metals
Major metal impurities	0.0011% Fe	0.23% Fe	0.41% Na, 0.32% Fe	31.8% Fe, 5.3% Na, 0.8% Mg
References	Cabot datasheet, Wang et al. 2010	Sargent et al. 2009; Wang et al. 2010; Mishra et al. 2012	Pacurari et al. 2008a; Porter et al. 2010; Mishra et al. 2012	Msiska et al. 2010

*Brunauer–Emmett–Teller nitrogen absorption method.

asbestos (Kim et al. 2012). In addition, toxicogenomic, protein and cell behavioural analyses can assist in phenotypically anchoring each particle with mechanisms promoting neoplastic transformation. By linking cell behaviours to genome expression signatures, chronic ENM exposure models would not only provide more relevant conditions to the real scenario, but their *in vitro* application also allows one to evaluate which physicochemical properties of nanomaterials elicit signalling mechanisms for potential neoplastic transformation.

Materials and methods

Preparation of dispersed particles

All tested particles were previously characterised by other studies and their physiochemical properties are summarised in Table I. Briefly, SWCNTs, synthesised using high-pressure carbon monoxide disproportionate process (HiPCO), were obtained from carbon nanotechnology (CNI, Houston, TX). SWCNTs were acid treated to remove a significant portion of metal catalyst contaminants. UFCB, SWCNT and MWCNT elemental analysis was performed using nitric acid dissolution followed by inductively coupled plasma-atomic emission spectroscopy while particle surface area was determined using Brunauer Emmet Teller nitrogen absorption-desorption technique at −196°C using a SA3100 Surface Area and Pore Size Analyzer (Beckman Coulter, Fullerton, CA, USA). Purified SWCNT contained less than 1% w/w of contaminants (Table I; Wang et al. 2011b). MWCNTs were provided by Mitsui & Company (MWNT-7, lot #05072001K28) containing 0.41% w/w metal impurity (Porter et al. 2010). Both SWCNTs and MWCNTs possessed ≤0.32% Fe and ≤0.41% Na ion impurities. Crocidolite asbestos (CAS# 12001-28-4) was originally obtained from the Kalahari Desert in South Africa by the National Institute of Environmental Health Sciences (Research Triangle Park, NC, USA). Crocidolite fibres had a mean length of 10 μm, mean diameter of 0.21 μm and surface area of 9.8 m^2/g (Msiska et al. 2010). Ultrafine carbon black (Elftex 12) was obtained from Cabot (Edison, NJ, USA) and contained <1% w/w metal impurities. All particles possessed surface areas between 9.8 and 43 m^2/g except for SWCNT which possessed 10–100-fold greater surface area (400–1040 m^2/g).

Particles were suspended in phosphate-buffered saline (PBS) to acquire stock solutions of 0.1 mg/ml. Next, a natural lung surfactant, Survanta (Abbott Laboratories, Columbus, OH, USA), was added to UFCB, SWCNT and MWCNT stock solutions to aid in their dispersion. The Survanta concentration in particle stock solutions was 150 μg/ml. All particles were dispersed using light sonication (Sonic Vibra Cell Sonicator, Sonic & Material Inc., Newtown, CT, USA) with the power, frequency and amplitude settings of 130 W, 20 kHz and 60% for 10 sec followed by dilution with cell culture medium to exposure dose. Final Survanta concentration in exposure medium was 0.15 μg/ml. Our Survanta dispersion method was previously optimised for improved dispersion of CNT and UFCB in cell culture media to mimic structure size distribution obtained by aerosolisation of dry CNT (Wang et al. 2010). Survanta exposure alone and dispersed UFCB does not cause acute cell proliferation or cytotoxicity; however, dispersed CNTs exhibited significant increases in both proliferation and cytotoxicity compared to non-dispersed agglomerated CNTs (Wang et al. 2010; Mishra et al. 2012).

Dimensions and imaging of dispersed particles in medium were determined using field emission scanning electron microscopy methods as previously described (Wang et al. 2010; Mishra et al. 2012). Briefly, dispersed particles were suspended in medium (0.02 μg/cm^2) and filtered through polycarbonate filter to collect dispersed particles. Dried samples were mounted, gold/palladium sputter coated and imaged at 400 and 30,000 magnification. Length and width measurements of >300 particles from three independent replicates were performed. Survanta-dispersed SWCNT structure exhibited mean count dimensions of 1.08 μm × 0.27 μm (Table I; Wang et al. 2010), while MWCNT structure exhibited 5.1 μm × 0.078 μm mean dimensions (Figure 1; Mishra et al. 2012). Since asbestos readily disperses in PBS with light sonication, no Survanta addition was performed. The same concentration of Survanta alone (0.15 μg/ml) and PBS alone were used as dispersant or saline (no treatment) controls.

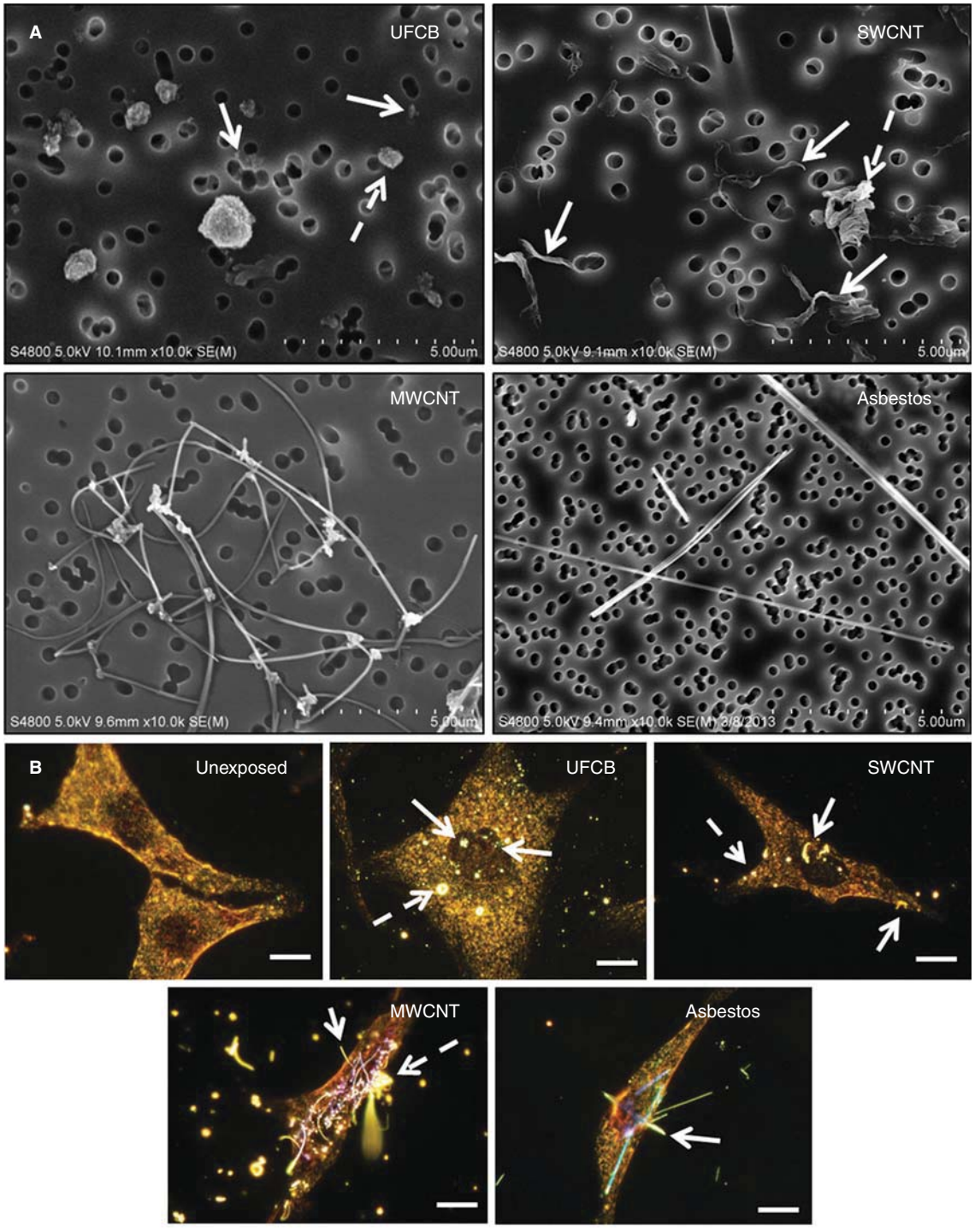

Figure 1. Visual characterisation of dispersed UFCB, SWCNTs, MWCNTs and crocidolite asbestos particle morphology and cellular fate in exposed human SAECs. A) Scanning electron microscope micrographs of dispersed particles. Dispersed UFCB (top left) and SWCNTs (top right) exhibited both nano-sized particles (white arrows) and micron-sized agglomerates (dashed arrow). MWCNTs (lower left) exhibited either single fibre or loosely tangled agglomerates while asbestos (lower right) existed as needle-like fibres. B) Hyperspectral dark-field microscopy micrographs of 24-h exposed SAEC to each dispersed particle. Cells were fixed and toluidine stained for contrast. Particles possess an intense white halo while stained cytoplasm and nucleus appears yellow and blue/purple, respectively. Nano-sized particles were co-localised to both cytoplasm and nucleus (solid while arrow) while micron-sized agglomerates were associated with cytoplasm or acellular (dashed white arrows). SWCNTs, MWCNTs and asbestos fibres were observed to penetrate and co-localise with both cytoplasm and nucleus. Bar = 10 μm.

SAEC culture and subchronic exposure

Primary human SAECs immortalised with hTERT were kindly provided by Dr. Tom Hei (Piao et al. 2005). SAECs were chosen as an ideal model since aspiration of CNT results in substantial deposition in terminal bronchioles and alveolar region of exposed mice (Mercer et al. 2010). SAECs were cultured in SABM medium supplemented with Clonetics SAGM SingleQuots (Lonza, Walkersville, MD, USA) which contained 0.4% v/v bovine pituitary extract, 0.1% insulin, 0.1% hydrocortisone, 0.1% retinoic acid, 1% bovine

serum albumin, 0.1% transferrin, 0.1% triiodothyronine, 0.1% epinephrine, 0.1% human epidermal growth factor and 0.1% gentamicin. Cells were cultured at 37°C in a humidified 5% CO_2 incubator during and following exposure.

SAECs were continuously exposed for 6 months to a sub-toxic dose (0.02 μg/cm^2, equivalent to 0.1 μg/ml) of dispersed UFCB, SWCNT, MWCNT or crocidolite asbestos in a six-well culture plate in triplicate. Each replicate was exposed and independently assayed throughout the study. This relatively low concentration was chosen due to its relevance to *in vivo* SWCNT and MWCNT exposure dose of 10 μg/mouse previously reported (Stone et al. 1992; Mercer et al. 2008; Porter et al. 2010). Every 3–4 days exposure media were removed, cells were triplicate washed with PBS and resupplied with media dosed with dispersed test particles. Cells were passaged weekly at pre-confluent densities using a solution containing 0.05% w/v trypsin and 0.5 mM EDTA (Invitrogen, Carlsbad, CA, USA). Parallel cultures grown in the same background concentration of dispersant or saline medium provided passage-matched controls and were designated as DISP and SAL cells, respectively. Following long-term exposure, particle-exposed cells were referred to as D-UFCB, D-SWCNT, D-MWCNT and ASB cells, respectively.

ENM cell uptake and fate determination

Suspended parental SAECs (2×10^4 cells) were seeded onto sterile glass coverslips into a 24-well plate overnight in triplicate. Cells were exposed to each dispersed particle (0.02 μg/cm^2) or unexposed medium for 24–48 h to evaluate cell uptake and co-localisation with major cell organelles. Following exposure, cells were fixed, stained and examined for cell/particle co-localisation under an Olympus BX-41 scope using dark-field enhanced microscopy (CytoViva, Auburn, AL, USA) using previously described methods (Mercer et al. 2011). Briefly, cells were PBS washed, fixed in 10% neutral buffered formalin, PBS washed again, stained with 0.1% w/v toluidine blue and rinsed thrice in distilled water. Stained cells were dehydrated in ethanol, cleared in xylene and mounted to glass slides with Permount. Since ENMs possess several attributes ideal for producing high quantities of scattered light (Mercer et al. 2011), enhanced dark-field microscopy images ENM scattered light compared to low amounts of scattered light from surrounding tissue.

Cell proliferation assays

All cell morphology, cancer hallmark behaviour and genome expression signature assessments were performed between 1 and 15 passages post-exposure (Table II). Immediately following 6-month exposure, suspended cells were seeded in duplicate at 1×10^5 cells/well in a 6-well plate and cultured up to 72 h to visually assess proliferation. Cells were then digitally photographed using reverse phase contrast on an Olympus IX70 inverted microscope equipped with a Retiga 2000R digital camera (QImaging, Surrey, BC).

Following exposure, colony-forming efficiency (CFE) was performed to assess cell proliferation using methods for MWCNT exposure (Ponti et al. 2012). Briefly, 300 cells were plated in triplicate to 60-mm plates (28.2 cm^2 growth area) and cultured for 7 days with one medium change occurring on Day 4. Surviving cells were washed in PBS, fixed in 4% paraformaldehyde, stained with 1% w/v crystal violet, rinsed twice with MilliQ water and allowed to dry. Plates with colonies were digitally photographed. Five independent experimental assays were performed. Colony counts were visually scored under an inverted scope and mean CFE calculated, where CFE (%) = (average treated cells/average of DISP cells × 100).

Starting at second passage post-6-month exposure, passage-matched treated and control cells were plated in sextuplicate in 100 μl normal growth medium to 96-well plate at 2×10^3 cells/well and incubated for 24–48 h. Next, 10 μl of WST-1 reagent was added to each well (Mishra et al. 2012) and spectrophotometrically assayed at 450 nm with SpectraMaxPlus 384 (Molecular Devices, Sunnyvale, CA, USA). To validate that increased mitochondrial activity correlated with live cell number, trypan exclusion assay was performed by seeding 1×10^5 cells in a 6-well plate in duplicate and incubating for 24 and 48 h. Next, cells were collected via trypsinisation, stained with trypan blue and counted using a Countess cell counter (Invitrogen). A minimum of three independent experiments were performed for both WST-1 and exclusion assays. Exclusion assay data were pooled across experiments prior to statistical analysis.

Cell morphological transformation assessment

A morphological transformation assay for foci was conducted based on previously described methods for MWCNT exposure (Ponti et al. 2012). Briefly, all six exposed cell types were seeded at 3×10^4 cells/dish to 60-mm plates in triplicate. Cells were cultured for 14 days with a PBS wash and fresh growth medium supplied every 3 days until a uniform monolayer was established. Following medium change at Day 14, cell medium was not changed for 1 week. On Day 21, cells were PBS washed, fixed in 10% formalin and stained with 1% crystal violet to visualise foci. The assay was repeated three times and Type III foci were scored from each treatment under an inverted microscope using cell transformation criteria described by Sasaki et al. 2012. Transformation frequency (TF) was calculated as TF = [foci count/(CFE (%) × seeding efficiency × cells seeded × replicate plates)].

Soft agar colony formation assay

All SAEC lines were assayed for anchorage-independent cell proliferation using a previously described soft agar assay method (Azad et al. 2010). Briefly, 0.5% w/v agar medium was obtained by mixing Difco agar, 15% v/v foetal bovine serum (FBS) and 1% gentamicin with 2× concentrate MEM medium (Lonza) at 44°C. Appropriate amounts of each growth factor from the SAGM SingleQuots kit (Lonza) that equalled their respective normal growth medium concentrations were added to the warm agar since all cell lines did not survive in preliminary soft agar assay trials. Next, all SAEC lines were suspended in 0.33% agar at 1×10^4 cells/well and slowly layered onto precast agar in triplicate into six-well plates. After 14 days incubation, colonies were examined and digitally photographed under light microscopy. Only colonies with >50 μm

Table II. *In vitro* assay conditions and endpoints used to assess neoplastic-like behaviour in human SAECs subchronically exposed to ultrafine carbon black, SWCNTs, MWCNTs and crocidolite asbestos.

In vitro assay	Available growth area (cm^2)	Seeding density	Duration	Endpoint
CFE	28.2	300	7 days	% of colonies
Morphological transformation	28.2	30,000	21 days	Foci count
Cell proliferation	0.33	5000	24 h, 48 h	WST-1 absorbance
Trypan exclusion assay (proliferation)	28.2	30,000	24 h, 48 h	Live cell count
Soft agar colony formation	9.6	10,000	14 days	Colony count
Invasion matrigel chemotaxis transwell	0.3	15,000	48 h	Invaded cell count
Migration chemotaxis transwell	0.3	30,000	24 h	Migrated cell count
HUVEC angiogenesis of SAEC conditioned medium	2.0	45,000	16 h	Tube node count
Whole-genome expression profile	28.2	1,000,000	24 h	mRNA expression

diameter were scored as positive in five replicate photographs per well. A minimum of three independent soft agar assays were performed.

Invasion and migration assay

Following exposure all exposed cells were subjected to chemotaxis Transwell invasion and migration assays (Azad et al. 2010). Invasion Matrigel Transwell inserts (8 μm pores; BD Biosciences) contained a thin layer of Matrigel to simulate extracellular matrix while migration control inserts (8 μm pores; BD Biosciences) did not. Briefly, cells were suspended in basal SABM medium without SingleQuot growth factors and seeded at 1.5×10^4 and 3×10^4 cells/insert into the upper chamber of preconditioned Transwell inserts for invasion and control inserts for migration, respectively. Duplicate inserts each containing 250 μl of cell suspension were immediately placed into individual wells containing 750 μl of normal SAEC growth medium in a 24-well plate. Invasion and migration assays were cultured for 48 or 24 h, respectively, to assess cell movement from upper to lower chambers. Next, a sterile cotton swab was used to remove all non-mobile cells from the inside of each insert. Adherent cells on underside of membrane of each insert were fixed, stained with Diff-Qik solutions according to manufacturer's instructions, rinsed in water and allowed to dry. Lastly, inserts were visualised in five random fields of view and scored under an inverted microscope. Three independent experimental runs were carried out for both assays.

Angiogenesis assay

Primary human vascular endothelial cells (HUVECs) were used to assay angiogenic potential of conditioned media from transformed cells using a two-dimensional angiogenic assay previously described (Azad et al. 2012). Briefly, low-passage parental SAECs and all six exposed cell types were plated at 5×10^5 cells/plate into 60-mm plates and held overnight. Next, cells were washed in sterile PBS and allowed to culture in 1 ml of fresh base SABM medium for 24 h. Conditioned medium was then removed from each cell line and frozen at −80°C until needed. HUVEC cells acquired from ATCC were cultured in MCDB 131 medium supplemented with 25% v/v heat-inactivated FBS, 0.05% bovine brain extract, 0.25% w/v endothelial growth factor, 0.1% heparin, 1% L-glutamine and 1% gentamicin. Sub-confluent HUVECs between second and seventh passage were suspended in a 1:1 ratio mix of SABM conditioned media and HUVEC reduced medium (2.5% dialysed FBS). HUVEC suspensions (4.5×10^4 cells/well) were seeded in duplicate onto reduced growth factor Matrigel-coated wells in 48-well plates. After 18 h, five replicate photos per well were digitally photographed and the number of endothelial cell tube nodes were scored. Three independent experimental runs were performed.

mRNA collection, reverse transcription and microarray hybridisation

To determine mechanisms of action driving CNT-driven neoplastic-like transformation, collected mRNA from all six exposed cell types at second passage post-exposure was subjected to whole-genome expression microarray analysis following MIAME guidelines. All exposed and passage control SAECs were seeded in triplicate at 5×10^5 cells to 60-mm plates in normal growth medium and incubated in normal growth conditions for 1–2 d. Then, sub-confluent plates were lysed with ice-cold TRIzol Reagent (Invitrogen) following manufacturer's instructions to collect mRNA. Lysates were then immediately frozen at −80°C for 24 h and shipped on dry ice to ArrayStar (Rockville, MD, USA) for mRNA processing, microarray hybridisation and probe expression normalisation. On arrival, mRNA was extracted following manufacturer's protocol and evaluated for RNA quality and quantity using a Bioanalyzer 2100 (Agilent) and Nanodrop ND-1000. mRNA was then reverse-transcribed with Superscript double-stranded-cDNA synthesis kit (Invitrogen). cDNA samples were then amplified, Cy3-labeled with NimbleGen one-colour DNA labelling kit and hybridised to NimbleGen whole human genome 12 × 135k microarrays in NimbleGen Hybridisation System. Following microarray plate image capture with Axon GenePix 4000B (Molecular Devices), images were uploaded into NimbleScan (v2.5), and Cy3 label intensities determined. Intensities were quantile normalised using Robust Multichip Average method included in NimbleScan. Only genes expressing ≥50.0 normalised intensity in all 18 samples were subjected to further analysis. All normalised gene expression data were deposited to NCBI Gene Expression Omnibus archive and are accessible via accession number (GenBank ID: GSE41178).

Differentially expressed genes and cluster analyses

Differentially expressed genes (DEGs) for each treatment were determined in Agilent GeneSpring GX (v11.5.1) by comparing each gene's normalised intensity to DISP SAEC

control intensity using a t-test ($\alpha = 0.05$) and a ±2.5-fold change screen. DISP SAECs served as an appropriate control since D-SWCNT, D-MWCNT and D-UFCB SAEC cells were exposed to lung surfactant and allowed for identification of particle-specific effects. Fold change and *p*-values for each DEG were saved in a tab-delimited text file for upload into Ingenuity pathway analysis (IPA) ver. 9.0 (Ingenuity Systems, Redwood City, CA, USA).

To further delineate whole-genome expression signature differences between treatments using cluster analysis techniques, normalised unscreened fold change data in a tab-delimited file were uploaded into MultiExperimental Viewer (Saeed et al. 2006). Due to the size of the data set, the lowest 20% of the least variable genes across all treatments were removed from the data set. Next, a one-way ANOVA ($\alpha = 0.05$) was used to identify genes whose expression differed among treatments. Both filters resulted in 20,497 probes for cluster analyses. Unsupervised hierarchical cluster analysis was performed on screened genes using Pearson's correlation and average linkage to develop a dendrogram and fold-change heat map. To validate the cluster analysis, the same screened data set was subjected to principal component analysis (PCA) to evaluate inter- and intra-sample clustering. The top three principal components were used to map all 18 samples in a three-dimensional space.

Ingenuity pathway analysis

DEG data from each treatment were uploaded into IPA for Core Analysis (Ingenuity Systems, Redwood City, CA, USA) to determine major alterations in cell functions, gene signalling networks (GSNs) and key genome alterations promoting neoplastic transformation in CNT-exposed cells. As previously described (Stueckle et al. 2012), negative logarithm *p*-values from IPA were used to rank cellular/molecular functions, disease functions, canonical pathways and signalling networks to identify potential genes and/or GSNs that promoted neoplastic transformation in D-SWCNT, D-MWCNT and ASB SAECs. Gene IDs, t-test *p*-values and fold expression data in tab-delimited text files were uploaded in IPA. Using IPA-generated negative logarithm *p*-values, score rankings were used to rank cellular/molecular functions, disease functions, canonical pathways and signalling networks to identify genes and novel signalling pathways potentially promoting observed neoplastic transformation. *P* values and GSN scores reflected likelihood tests of a gene occurring in a given pathway versus other pathways based on pure chance. Z scores (≥±2) were used to make predictions of activation/inhibition of cellular functions, respectively.

To determine potential novel signalling mechanisms and identify differences between CNT- and asbestos-induced tumour-promoting signalling, IPA-generated *p* values and GSN scores were determined, which reflected likelihood tests of a gene occurring in a given pathway versus other pathways based on pure chance. Initial evaluation of IPA functions and networks identified cancer-related disease and gene signalling functions in CNT-exposed cells. Therefore, ranked GSNs were mapped and cancer-related genes and signalling pathways were identified. To further depict cancer-related signalling, CNT cancer GSNs were created by filtering the DEG data set for those genes with a cancer-related role. Lastly, cancer cells typically exhibit increased proliferation, tumour formation, migration, invasion and anti-apoptosis abilities. Cell behaviour GSNs (i.e. pro-cancer GSN) were developed for each of these phenotypes to assist in identifying signalling patterns. Genes passed the filter if they promoted the behaviour and were up-regulated or antagonised the behaviour and were down-regulated.

rtPCR confirmation of microarray expression

To confirm microarray gene expression data, a subset of key genes of interest was selected to validate their mRNA expression. 5×10^5 cells from each treatment were seeded in 60-mm^2 dishes and allowed to proliferate for 1–2 days. mRNA from sub-confluent cells was collected via TRIzol procedures (described above) and stored for 48 h at −80°C prior to rtPCR analysis. Intron-spanning primers and probes were designed using ProbeFinder 2.45 (Roche) and obtained from Operon (Table S1). RNA sample quality was assessed using NanoDrop 1000 (Thermo Scientific), reverse transcribed, and amplified using 2720 Thermo Cycler (Applied Biosystems) in triplicate. Quantitative rtPCR was conducted on an ABI 7500. Each thermocycling reaction used 25 µl total volume containing 7.25 µl cDNA, 2.5 µl primers and 12.5 µl Roche Taqman Master Mix. Relative expression levels to *GAPDH* were determined using $2^{-\Delta\Delta ct}$ and compared to microarray values using a t-test.

Western blot analysis

Following 6-month exposure, cells were incubated in lysis buffer containing 20 mM Tris–HCl (pH 7.5), 1% Triton X-100, 150 mM NaCl, 10% glycerol, 1 mM Na_3VO_4, 50 mM NaF, 100 mM phenylmethylsulfonyl fluoride and a commercial protease inhibitor mixture (Roche Molecular Biochemicals) at 4°C for 20 min. The lysate was collected and determined for protein content using the Bradford method (Bio-Rad Laboratories, Hercules, CA, USA). Proteins (40 µg) were resolved under denaturing conditions by 10% sodium dodecyl sulphate-polyacrylamide gel electrophoresis and transferred onto nitrocellulose membranes (Bio-Rad). The transferred membranes were blocked for 1 h in 5% nonfat dry milk in TBST (25 mM Tris–HCl, pH 7.4, 125 mM NaCl, 0.05% Tween 20) and incubated with the appropriate primary antibodies at 4°C overnight. p53, IL-1B and IL8 anti-bodies were purchased from Santa Cruz Biotechnology (Santa Cruz, CA, USA) while all other antibodies were acquired from Cell Signaling Technology (Danvers, MA, USA). Membranes were washed twice with TBST for 10 min and incubated with horseradish peroxidase-coupled isotype-specific secondary antibodies (Santa Cruz) for 1 h at room temperature. The immune complexes were detected by enhanced chemiluminescence detection system (Amersham Biosciences, Piscataway, NJ, USA) and quantified using analyst/PC densitometry software (Bio-Rad Laboratories, Hercules, CA, USA).

Statistical analyses

DISP cells served as negative passage control for both cell behaviour and microarray statistical comparisons among

treatment groups. All cell behaviour assay data were pooled from three independent exposure replicates and analysed using one- or two-way ANOVA ($\alpha = 0.05$) to determine differences between chronic exposure treatment groups. Post hoc Tukey–Kramer honestly significant difference tests were used to identify those treatments that were different from each other. Microarray and rtPCR mRNA expression values for each gene were compared using a two-way Student's t-test. All statistical analyses were performed in JMP 9.0 (SAS Institute).

Results

Nanoparticle and asbestos uptake in SAECs

Scanning electron microscopy displayed dispersed particles before exposure (Figure 1A) while hyperspectral dark-field visualisation of 24-h-exposed SAECs showed that dispersed UFCB co-localised in both the cytoplasm and nucleus (Figure 1B). Dispersed SWCNT, MWCNT and asbestos exhibited fibre-like morphologies either co-localised in the cytoplasm of cells or puncturing the cellular or nuclear membranes. UFCB, SWCNT and MWCNT also formed large micron-sized aggregates that appeared to make contact with the cell membrane. Adjustment of the focal plane to acquire Z-stack images (data not shown) suggested that these large micron-sized particles were potentially lying on top of cells and not within the cytoplasm. At equal cell seeding density, more dispersed SWCNT and MWCNT particles were observed co-localised with SAECs than asbestos fibres.

Subchronic exposure to D-SWCNT, D-MWCNT and asbestos alters cell growth and morphology

After 24 weeks of exposure, D-SWCNT and D-MWCNT cells visually exhibited greater proliferation over 48 h (Figure 2A). Both D-SWCNT and D-MWCNT exhibited significantly greater CFE (Figure 2B) and morphological transformation evidenced by Type III foci than DISP control cells (Figure 2C). Parental SAECs possessed significantly lower CFE than all other cells. Type III foci exhibited deep basophilic staining, multilayered mounding with different cell orientations and invasive growth at colony edges. Both D-CNT SAECs demonstrated cells with numerous intracellular vesicles compared to DISP and SAL control cells while ASB periodically displayed this morphological characteristic. Attempts to identify these vesicles by staining lipid droplet, endoplasmic reticulum, Golgi apparatus, lysosome and peroxisome were all negative (Figure S1). In addition, all six passaged cell lines possessed pleomorphic giant cells possibly due to long-term passage. In summary, increased CFE, morphological transformation and visual observations of altered morphology suggested a moderate CNT-induced lung epithelial morphological transformation.

Chronic SWCNT and MWCNT exposure induces a more aggressive neoplastic-like transformation phenotype than asbestos exposure

Cancer hallmark transformation phenotypes of the particle-exposed cells were determined by several well-established methods and compared to passaged DISP control cells. D-SWCNT, D-MWCNT and ASB cells exhibited significantly greater cell proliferation at 48 h compared to SAL, DISP and D-UFCB cells (Figure 3A-1). Similarly, D-SWCNT, D-MWCNT and ASB cells showed a significant increase in live cell number over 48 h compared to SAL and DISP controls. D-UFCB cells displayed a significantly lower number of cells compared to controls indicating a reduced ability to attach and proliferate following chronic UFCB exposure (Figure 3A-2). A 2-week proliferation analysis during subchronic exposure showed that D-UFCB cells recovered by 72 h post-seeding, but exhibited lower viable cell counts at 7 days post-seeding than all other treatments (Figure S6).

Next, anchorage-independent cell growth was determined by assessing the number of isolated colonies on soft agar to confirm SWCNT- and MWCNT-induced neoplastic-like transformation compared to asbestos. D-SWCNT, D-MWCNT and ASB SAECs exhibited significant increases in number of colonies formed compared to control SAECs (Figure 3B). D-SWCNT and D-MWNCT SAECs displayed a 2.2-fold increase compared to DISP control cells, while ASB-SAECs had a significant 1.3-fold increase in formed colonies over SAL control cells.

To test for enhanced cell motility, all subchronic SAEC lines were assessed for invasion and migration ability. Both D-SWCNT and D-MWCNT cells demonstrated a significant 4.7-fold increase in 48-h cell invasion and a 2–2.5-fold increase in 24-h cell migration as compared to the control cells (Figure 3C and Figure S2). ASB SAECs showed a significant increase in invasion ability but no significant change in migration ability compared to DISP cells.

Lastly, we assessed angiogenic potential of D-UFCB, D-SWCNT, D-MWCNT and ASB SAECs compared to parental, SAL and DISP control SAECs. Conditioned media from D-SWCNT, D-MWCNT, ASB and SAL SAECs caused a significant increase in tube formation while UFCB and parental SAECs exhibited a significant decrease compared to DISP SAECs (Figure 3D). Increased angiogenic potential in SAL cells compared to DISP control cells was possibly due to increased mRNA expression of *HIF1α*, *VEGF* and p65 NF-κB (microarray data described below) which was not observed for CNT-exposed cells. In summary, the increased expression of several cancer hallmarks (i.e. cell proliferation, soft agar colony formation, migration, invasion and angiogenesis) in both D-SWCNT- and D-MWCNT-exposed cells suggests that subchronic CNT exposure elicits a more aggressive epithelial lung cell neoplastic-like transformation effect than asbestos, suggesting increased risk for CNT-induced carcinogenesis.

D-SWCNT and D-MWCNT SAECS display substantially different genome signatures from asbestos SAECs

To assess potential neoplastic-like transformation mechanisms and to compare genome expression signatures of SAECs subchronically exposed to CNTs vs. asbestos, collected mRNA from all exposed and control SAECs were subjected to whole-genome expression microarray profiling. Following mRNA hybridisation and DEG determination, hierarchical clustering (HC) heat map expression signature and PCA showed that D-SWCNT- and D-MWCNT-transformed SAECs possessed the most similar toxicogenomic signatures, which were clearly

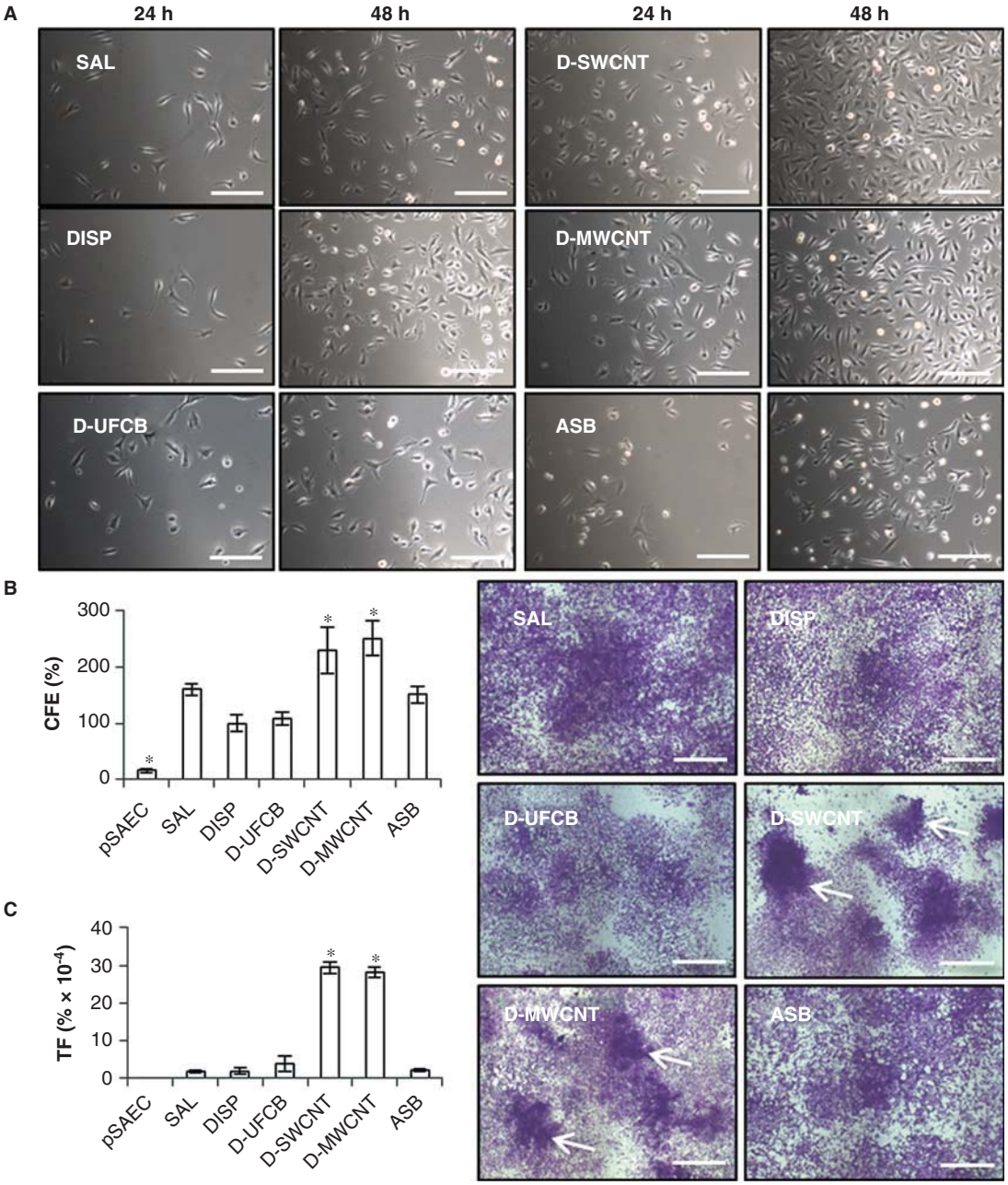

Figure 2. Altered proliferation and morphological transformation in SAECs subchronically exposed (6 months) to dispersed SWCNTs, dispersed MWCNTs or crocidolite asbestos. A) D-SWCNT and D-MWCNT cells showed greater density of cells at 48 h post-seeding than all other treatments. Bar = 500 μm. B) D-SWCNT and D-MWCNT cells possessed significantly greater CFE than DISP control and all other treatments while parental SAECs (pSAEC) exhibited low efficiency. C) D-SWCNT and D-MWCNT cells exhibited higher TF than all other treatments based on Type III foci counts (left). Type III foci (right; white arrows) exhibited deep basophilic staining, multi-layered cell growth and invasive growth into monolayer. All other groups demonstrated Type I foci with SAL and ASB cells occasionally displaying Type II foci. Bar = 1 mm.

distinct from ASB cells (Figures 4A and B). In addition, DISP and D-UFCB SAECs showed similar expression signatures, which were loosely clustered with ASB SAECs. Conversely, SAL SAECs possessed a unique expression signature, which differed from all other cell lines. PCA explained 75.8% of the variance in the first three components and confirmed the HC analysis of treated SAECs.

D-SWCNT and D-MWCNT SAECs experienced altered cell death, proliferation, mobility and development signalling

To identify signalling pathways associated with CNT-induced potential neoplastic-like transformation compared to asbestos, all DEG data were subjected to IPA Core Analysis. Top-ranked cellular/molecular functions, disease functions and signalling networks were used to identify GSNs contributing to a potential neoplastic-like transformation phenotype. Both D-SWCNT and D-MWCNT SAECs displayed large alterations in DEGs associated with cell proliferation, movement, cell death, development and cell–cell signalling (Figure 5A). Cell development signalling associated with connective tissue development was predicted as activated in D-SWCNT SAECs (*, $Z \geq 2$). Further analysis of the cell death function revealed that a large majority of the altered DEGs were associated with apoptosis. In addition, a majority

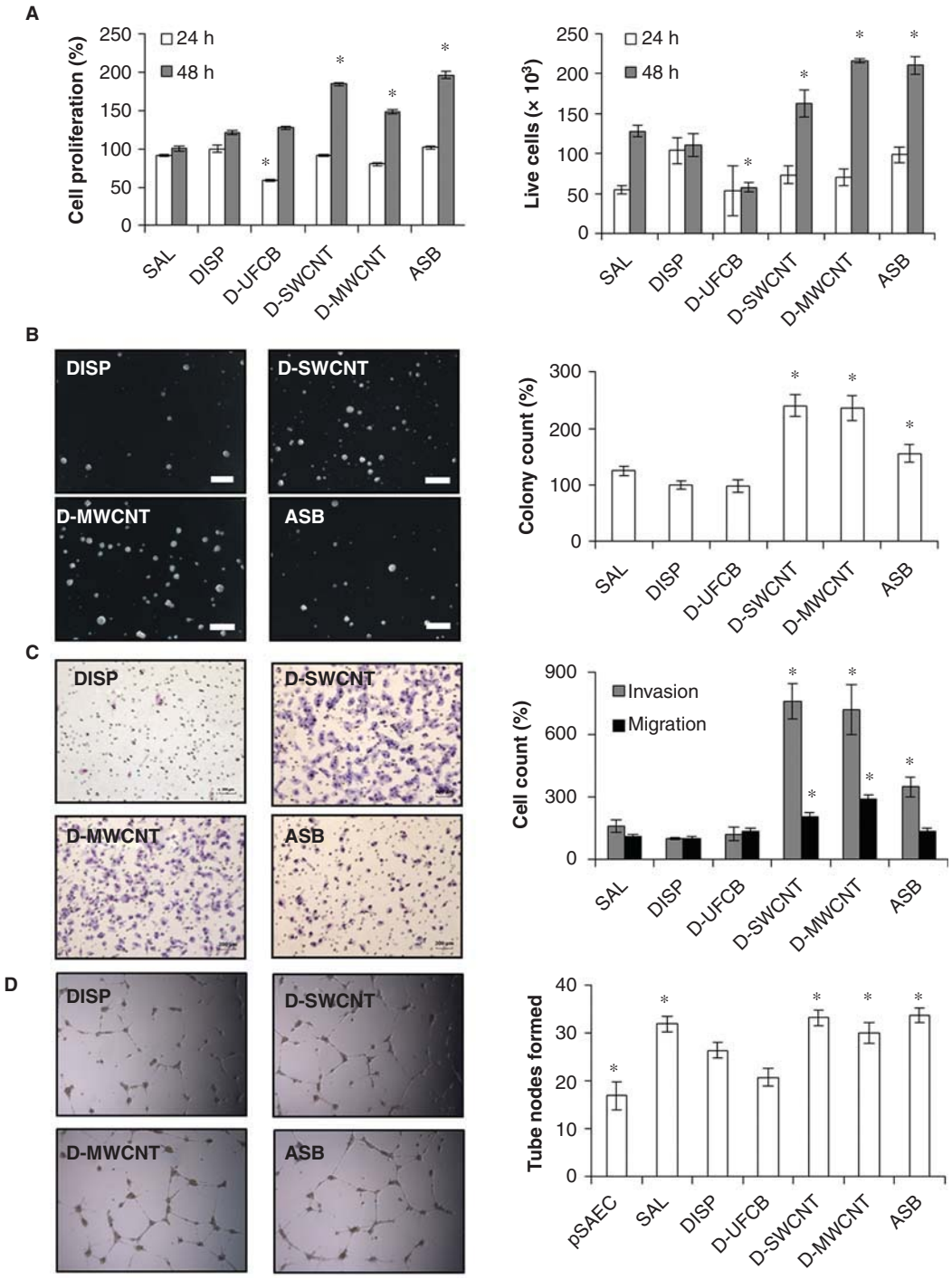

Figure 3. Subchronic exposure (6 months) to dispersed SWCNTs, MWCNTs and asbestos results in neoplastic-like transformation of SAECs compared to DISP control cells. A-1) Increased WST-1 proliferation activity, A-2) trypan blue exclusion cell number and B) soft agar colony formation in D-SWCNTs, D-MWCNTs and ASB cells compared to control cells. C) D-SWNCT and D-MWCNT cells possessed significantly greater Matrigel invasion and Transwell migration ability in growth factor-free medium than control and ASB cells. D) Enhanced angiogenesis tube formation behaviour of HUVEC cells exposed to conditioned media from D-SWCNT, D-MWCNT, ASB and SAL cell lines. Parental SAECs (pSAEC) displayed significantly lower angiogenic ability than DIPS cells. Columns with error bars represent mean ± SE. Three or more independent experiments were performed for each assay. * indicate significant difference vs. non-treated control.

of cell movement and development signalling in both D-SWCNT and D-MWCNT was associated with decreased gene expression of inflammatory cytokines and chemokines involved with leukocyte recruitment (†; $Z \leq -2$). ASB SAECs showed similar pattern in cell-death- and proliferation-related DEGs. Upon further analysis of those functions predicted as activated in ASB (*), a majority of these genes were associated with cell function (phagocytosis), inflammatory signalling and leukocyte cell functions. SAL cells exhibited changes in cell proliferation, death and development with predicted activation of endothelial cell development (*). Lastly, D-UFCB cells possessed large changes in cell proliferation, cell assembly, cell function and cell death signalling with a majority of these genes down-regulated. Cell invasion/

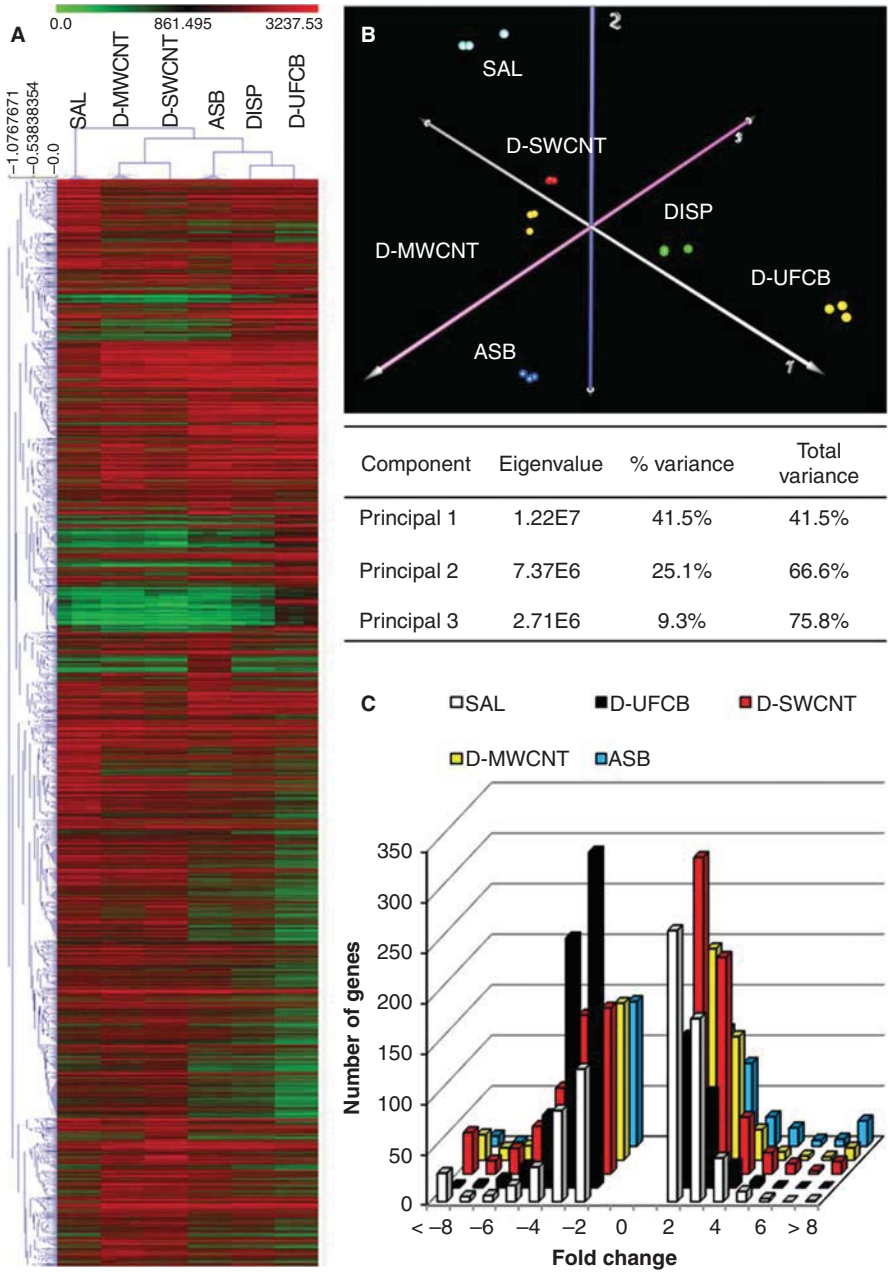

Component	Eigenvalue	% variance	Total variance
Principal 1	1.22E7	41.5%	41.5%
Principal 2	7.37E6	25.1%	66.6%
Principal 3	2.71E6	9.3%	75.8%

Figure 4. Unsupervised hierarchical cluster (HC) and principal component (PC) analysis of DEGs from cells subchronically exposed (6 months) to dispersed CNTs, asbestos and UFCB. A) D-SWCNT and D-MWCNT cells possessed similar genome expression signatures and differed substantially from asbestos-exposed, ultrafine carbon black and vehicle control signatures. B) PC analysis validation of HC analysis displaying differences between particle-exposed SAECs. C) Histogram comparison of up- and down-regulated DEGs compared to DISP control cells.

migration, cell proliferation, neoplasia and cell attachment signalling were predicted as inhibited (†) while cell death/senescence and homing of phagocytes/neutrophils were predicted as activated (*, Figure 5A).

Subchronic exposure to SWCNT and MWCNT altered gene expression, inflammation-related signalling and lipid metabolic signalling

In evaluating top-ranked molecular functions, D-SWCNT cells exhibited significant alterations in gene expression, post-translational modification and lipid metabolism (Figure 5B). D-MWCNT showed the most significant alterations to gene expression and predicted activation of lipid metabolism/transport (*). Conversely, ASB cells displayed a 2–5-fold decrease in DEGs associated with gene expression and a comparable number of post-translational modification, small molecule metabolism and transport DEGs to D-MWCNT. SAL and D-UFCB cells exhibited the largest number of DEGs in gene expression. Only D-UFCB and ASB cells possessed a substantial number of DEGs associated with DNA recombination and repair. ASB SAEC post-translational modification, amino acid metabolism, antigen presentation and molecular transportation were all predicted as activated (*). In summary, HAR fibres showed similar alterations in cellular functions, but exhibited strikingly different molecular functions, which were primarily driven by differences in lipid metabolism and inflammatory signalling.

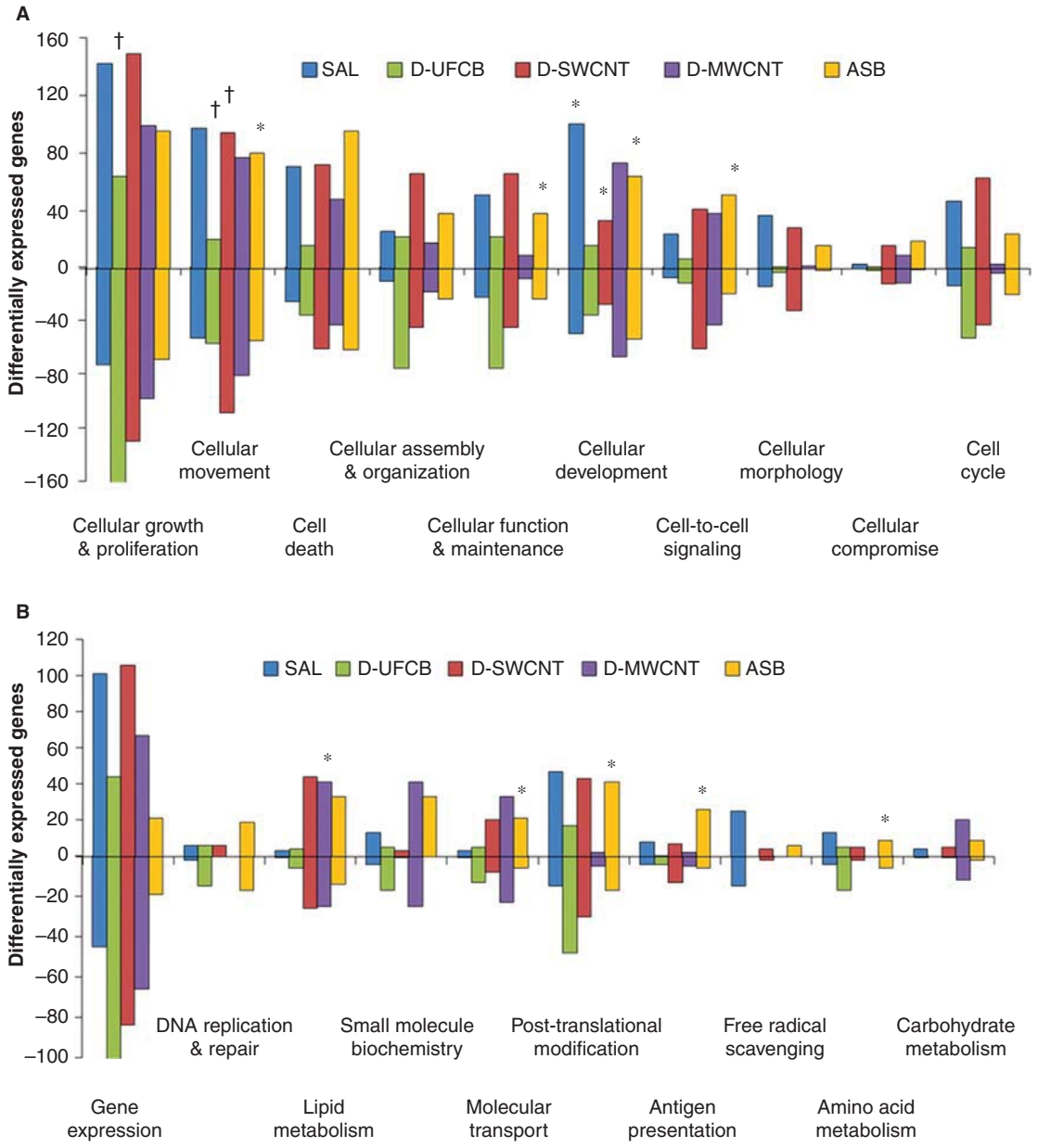

Figure 5. Top-ranked (*p*-value) altered A) cellular and B) molecular functions in CNT, asbestos, UFCB and saline control SAEC cells following subchronic exposure. Numbers of up- and down-regulated DEGs for each function are shown. All treatments were compared to dispersant-only control (DISP) expression. * and † indicate those functions that were predicted as activated or inhibited ($Z \geq \pm 2$), respectively.

Subchronic CNT exposure altered TNFR signalling, reduced immune response and altered cancer-related canonical pathways

To further uncover altered signalling pathways, top-ranked disease functions and canonical pathways were investigated for promotion potential of neoplastic-like phenotype. Cancer was the top-ranked disease for all five cell lines compared to DISP control cells (Table S2); however, genetic disorder was pronounced for both D-SWCNT and D-MWCNT genome expression signatures. All top-ranked organ system diseases were specific cancer types for all exposure treatments except ASB cells. Inflammatory response, arthritis disease and immunological disease were highly ranked in ASB cells, but were absent from top-ranked CNT disease functions. IPA predicted cancer inhibition (†) in D-UFCB cells while it predicted activation (*) of inflammatory response/disease in ASB cells. Investigation of top-ranked canonical pathways revealed that D-SWCNT SAECs exhibited changes in altered apoptotic, decreased inflammatory (*NFKB2*, Ikk) and cancer-related signalling (Table III). For both D-SWCNT and D-MWCNT cells, *CASP2*, *CASP3* and *CASP8* were over-expressed, while pro-apoptotic *BID*, *BAD* and *HTRA2* were under-expressed, thus suggesting altered apoptosis signalling. Down-regulated p100/p52 NF-κB (*NFKB2*) was a common player in many of the top-ranked canonical pathways for both D-SWCNT and D-MWCNT. D-MWCNT showed similar rankings; however, down-regulation of many genes in the complement system (*BF*, *C3b*, *C4b*; over-expressed *CD55*) and chemokines in IL-17 signaling (*CXCL1–3*, *IL8*, *CCL2*) took precedence. Conversely, ASB SAECs exhibited altered fibrosis, TREM and clathrin-mediated endocytosis signalling. Increased NF-κB inflammatory fibrosis

Table III. Top-ranked canonical signalling pathways for saline (SAL), D-UFCB, D-SWCNT, D-MWCNT and ASB-exposed SAECs compared to dispersant-only exposed cells.

Ingenuity canonical pathways	−log(*p*-value)	Ratio (%)
SAL		
Hepatic fibrosis/hepatic stellate cell activation	6.46	15.0
Role of macrophages, fibroblasts and endothelial cells in rheumatoid arthritis	5.37	9.9
IL-6 signalling	4.07	14.0
Role of osteoblasts, osteoclasts and chondrocytes in rheumatoid arthritis	3.63	9.6
Renin–angiotensin signalling	3.61	12.1
GNRH signalling	3.60	11.0
Xenobiotic metabolism signalling	2.96	8.6
Atherosclerosis signalling	2.95	11.2
CD27 signalling in lymphocytes	2.70	14.0
LPS/IL-1-mediated inhibition of RXR function	2.68	8.7
D-UFCB		
Hepatic fibrosis/hepatic stellate cell activation	2.74	11.6
Differential regulation of cytokine production in macrophages and T helper cells by IL-17A and IL-17F	2.63	27.8
Mitotic roles of polo-like kinase	2.23	14.1
Wnt/β-catenin signalling	2.20	10.3
Basal cell carcinoma signalling	1.81	12.3
Factors promoting cardiogenesis in vertebrates	1.64	10.5
D-SWCNT		
TNFR1/TNFR2 signalling	5.76	26.4
CD27 signaling in lymphocytes	4.01	21.1
Death receptor signalling	3.98	20
Chronic myeloid leukaemia signalling	3.86	16.2
LPS-stimulated MAPK signalling	3.56	17.1
14-3-3-mediated signalling	3.55	15.8
Angiopoietin signalling	3.39	17.6
Myc-mediated apoptosis signalling	3.37	19.7
4-1BB signalling in T lymphocytes	3.34	23.5
Apoptosis signalling	3.14	15.6
D-MWCNT		
Complement system	3.24	20
Role of IL-17A in arthritis	3.17	14.3
TNFR1 signalling	2.98	15.1
Aminosugars metabolism	2.76	9.17
Type II diabetes mellitus signalling	2.61	8.75
Atherosclerosis signalling	2.57	10.3
LXR/RXR activation	2.55	10.8
PTEN signalling	2.5	9.68
TWEAK signalling	2.48	15.4
LPS/IL-1-mediated inhibition of RXR function	2.48	8.22
ASB		
Hepatic fibrosis/stellate cell activation	8.08	13.6
TREM1 signalling	5.30	15.2
Clathrin-mediated endocytosis signalling	4.25	8.7
Complement system	4.23	20.0
CTLA4 signalling in cytotoxic T lymphocytes	3.99	11.2
Leukocyte extravasation signalling	3.97	8.50
Virus entry via endocytic pathways	3.82	11.0
NF-κB signalling	3.74	8.52
Axonal guidance signalling	3.68	6.0
MSP-RON signalling pathway	3.31	13.7

signalling was evident resulting in increased cytokine expression (*IL8*, *CCL2*). Over-expressed *ITGB2, SRC* and *PI3K* with under-expressed clathrins indicated an integrin-mediated uptake of asbestos fibres. Over-expressed interleukins, toll-like receptors and phospholipase C (e.g. *IL1B*, *TLR2, PLCγ2*) indicated activation of NF-κB inflammatory signalling. Surprisingly, several complement proteins down-regulated in CNT-exposed cells were also down-regulated in ASB cells. SAL cells possessed over-expressed fibrosis signalling (*COL1A1*, *PDGFRα/β*, *FGFR*, *VEGF*, *MMP2*) and inflammation (*IL6*, *IL8*, *RELA*, *MCP-1*) that dominated a majority of the top-ranked pathways. Conversely, D-UFCB demonstrated down-regulation of fibrosis (*TGFBR1*, *SMAD2*, *IL6*, *VEGF*, *CSF1*, *CCL2* and *MMP2*), WNT pathway and polo-like kinase signalling

(*APC*, *CCNB2*, *PLK*, *SLK*) indicating a reduced ability to proliferate and contribute to a particle-induced fibrotic response. In summary, both D-SWCNT and D-MWCNT SAECs exhibited altered apoptosis signalling, cancer-related signalling and decreased inflammatory signalling, which differed from ASB and SAL SAEC pro-inflammatory signalling.

Gene signalling analysis reveals cancer-associated signalling in D-SWCNT and D-MWCNT cells which differed from ASB cell signalling

Evaluation of top-ranked GSNs revealed several gene hubs known to exhibit pro-cancer or tumour-associated signalling in both D-SWCNT and D-MWCNT (Table IV). Ap-1 (*FOS*)-, *MYC*-, *NFKB2*-, *PPARG*- and *INHBA*-centred GSNs were common in both D-SWCNT and D-MWCNT SAECs promoting altered gene expression, lipid metabolism, cell proliferation and cell movement. Although more associated with D-MWCNT, both D-CNT SAECs displayed GSNs with altered actin, tubulin and collagen expression, suggesting a remodelling of intra- and extracellular structure and function. In addition, several GSNs centred on altered histone expression (e.g. histone deacetylases, histones 1 and 3), suggesting either epigenetic modifications and/or alterations to chromosome structure and integrity. ASB SAECs exhibited a drastically different ranked GSN profile compared to both D-CNT SAECs. ASB cells exhibited over-expressed *SRC*, *SPI1*, *TREM1* and NF-κB signalling with decreased hCG and *PRKACB* GSN hubs associated with cell assembly/maintenance, molecular transport, inflammatory response and cell–cell signalling. SAL SAECs exhibited a few similar expression profiles of several genes (Table IV; e.g. over-expressed *FOS*); however, over-expression of *RELA* and *TP53* in SAL SAECs appeared to dominate several top-ranked SAL GSNs. Top-ranked GSNs in D-UFCB highlighted decreased cell development (*GAS7*), cell maintenance, lipid metabolism and cell cycle (*TP53*). With a lack of neoplastic-like transformation behaviour, the SAL SAECs appeared to undergo a moderate *in vitro* non-neoplastic transformation associated with increased p53 and inflammatory NF-κB signalling following 6 months of continuous passage.

GSN analysis reveals distinct CNT pro-cancer signalling which differs from pro-inflammatory signalling in ASB cells

Based on aggressive neoplastic-like transformation phenotype and identification of several signalling pathways associated with carcinogenesis, cancer-associated GSNs were constructed in IPA to further identify potential complex signalling pathways in both D-SWCNT and D-MWCNT compared to ASB SAECs. Large complex pro-cancer networks for both D-SWNCT and D-MWCNT were characterised by proliferation, tissue development, cell movement and suppressed immune signalling, while ASB cell signalling was primarily driven by pro-inflammatory signalling (Figures S3–S5). By applying a strict filter to show only gene expression solely promoting cancer, D-SWCNT pro-cancer GSN revealed over-expressed *NRAS*, *MYC*, *FOS*, *CASP8*, *COL18A1*, *CDKN2A* and under-expressed *CSF2*, *CCL2* hub genes associated with cell proliferation and tissue morphology (Figure 6A). D-MWCNT pro-cancer GSN revealed a smaller network centred on over-expressed *MYC* associated with cell proliferation and cell movement (Figure 6B). Conversely, the ASB SAEC pro-cancer GSN possessed over-expressed *IL1B*, *SPI1*, *CASP8*, *CD44*, several inflammatory chemokines, including *CCL2*, *IFNA21*, and *BCL2L11,* with under-expressed *CXCL2*, *FN1*, *MMP2* and *CSF1* (Figure 6C). Cell proliferation, cancer and tissue morphology behaviour were associated with the ASB pro-cancer GSN. In summary, subchronic D-SWCNT and D-MWCNT exposure resulted in cancer-promoting signalling profile with known oncogenes in SAECs which differed from a pro-inflammatory signalling prolife in asbestos-exposed SAECs.

mRNA and protein expression validation of key tumourigenic signalling molecules

Following IPA analysis and identification of hub genes associated with potential tumourigenesis, a subset of key signalling molecules of interest for D-SWCNT, D-MWCNT and ASB cells were chosen to further investigate whether their protein expression matched the microarray and their potential as key players contributing to lung epithelial cell neoplastic-like transformation and potential lung carcinogenesis. rtPCR validation (Figure 7A) confirmed a majority of microarray expression values of key genes. Other significantly different rtPCR values were noted but were either over- or under-expressed in large magnitude, which matched the expression trends in the microarray.

Western blot analysis showed that D-SWCNT, D-MWCNT and ASB possessed over-expressed cFOS, c-Myc and PPARγ levels (Figure 7B), while the tumour suppressors Inhibin α and p53 were under-expressed (Figure 7C). We probed for p-p53 to evaluate if the p53 decrease was a function of loss of phosphorylation at serine 15 previously shown for SWCNT-transformed lung epithelial cells (Wang et al. 2011b). P-p53^{Ser15} levels were increased above SAL, DISP and D-UFCB levels, suggesting partial protection against p53 proteasomal degradation in D-SWNCT, D-MWCNT and ASB SAECs. Given caspase 8's prominence in the GSN analyses and known roles in cancer signalling, blots for pro-caspase 8 (57 kD) showed over-expression in D-SWCNT, D-MWCNT and ASB compared to both SAL and DISP control cells. Over-expression of N-terminal cleavage product (43 kDa) above pro-caspase 8 levels was apparent across all cell types except D-UFCB cells. Active caspase 8 (18 kDa) was not detected in any cell types. Next, we evaluated the status of NF-κB levels in the CNT- and ASB-transformed SAECs to evaluate whether differences between ASB and CNT inflammatory signalling were partially due to NF-κB expression. Both p100 and p52 *NFKB2* subunits were diminished in D-MWCNT and ASB cells compared to SAL and DISP cells (Figure 7D). D-SWCNT cells exhibited a substantial reduction in the p100 subunit compared to all other cell types. In agreement with microarray data, we found that both SAL and DISP had greater p65 NF-κB (*RELA*) levels than D-SWNCT, D-MWCNT and ASB cells. In addition, increased phosphorylation of IKKα/β was found in both D-SWCNT and D-MWCNT, suggesting degradation of NF-κB. To evaluate potential pro-inflammatory signalling in ASB cells, we evaluated protein expression for several key

Table IV. Top-ranked GSN with gene hubs and functions for saline (SAL), D-UFCB, D-SWCNT, D-MWCNT and ASB cells compared to dispersant-only-exposed human SAECs.

Gene hub *,†,‡	IPA functions	Score
SAL		
RELA↑	Cell death, embryonic development, immunological disease	38
PRKCA↑, Histone h3	Ophthalmic disease, metabolic disease, psychological disorders	36
CEBPA↑, PTPN6↓, peptidylpropyl isomerases↑↓	Connective tissue development, tissue development, gene expression	36
VHL↑	Post-translational modification, drug metabolism, molecular transport	36
VEGFA↑, FOXO1↓	Organ morphology, nervous system development, cardiovascular system development	36
Akt	Embryonic development, tissue development, developmental disorder	34
FOS↑	Gene expression, genetic disorder, metabolic disease	32
Caspases 2/8↑, VIM↑, PLA2G4A↑	Cardiovascular system development, cell morphology, carbohydrate metabolism	32
TP53↑, RELA↑, MMP2↑	Genetic disorder, skeletal and muscular disorders, cellular proliferation	31
PTK2↑, Cadherins↑, Collagens↑↓	Cellular movement, connective tissue disorders, genetic disorder	28
D-UFCB		
GAS7↑, MAPK6↓, SF3A1	Cellular organisation, RNA post-translational modification, cellular development	47
TP53↓	Lipid metabolism, small-molecule biochemistry, cell cycle	40
NR3C1↓, NFYB↓, RNA polymerase	Amino acid metabolism, small-molecule biochemistry, genetic disorder	38
Akt, CAV2↓	Cellular organisation, cell signalling, cellular maintenance	36
NFκB complex	Cell signalling, amino acid metabolism, cellular organisation	34
Histone H3↑, Histone 4	Infection mechanism, cellular development, cellular proliferation	34
Erk 1/2, PPP2R5C↓	Cancer, reproductive system disease, nervous system function	28
Jnk, Msn↓	Cancer, reproductive system disease, cell morphology	28
SHH↑, RUNX2↓, Mapk↓	Cell cycle, cellular proliferation, connective tissue disorders	28
CSF2↑, CSF1↓, BCL2↑, STAT5	Lymphoid tissue structure, organ development, cellular development	28
D-SWCNT		
FOS↑	Amino acid metabolism, small-molecule biochemistry, drug metabolism	40
ARRB1↑, INHBA↓, SMAD5↑, ID2↓	Gene expression, genetic disorder, liver cirrhosis	38
Vegf, Fsh, Ap1↑	Cellular proliferation, haematological function, carbohydrate metabolism	34
NFKB2↓	Lipid metabolism, molecular transport, small-molecule biochemistry	32
PPARG↑, LIF↓, SATB1↓	Cellular movement, embryonic development, reproductive function	32
MYC↑	Amino acid metabolism, drug metabolism, small-molecule biochemistry	32
FOXO1↑, Insulin, RXR retinoic acid	Cardiac enlargement, organ morphology, cellular proliferation	28
Clathrins↑↓, AMPH↓, Erk1/2	Infection mechanism, infectious disease, cancer	28
Jnk↑, C1QBP↑, Snare↑↓	Dental disease, cell death, auditory disease	28
POU5F1↓, UBE2D1↑, Ubiquitin	Nervous system function, tissue development, RNA damage and repair	27
D-MWCNT		
NFKB2↓	Lipid metabolism, molecular transport, small-molecule biochemistry	40
MYC↑, TAL1↓, CDC42↓	Cancer, haematological disease, immunological disease	36
Ck2, PPARG↑, Rxr	Lipid metabolism, molecular transport, small-molecule biochemistry	35
Actin↓, FOXA2↓, G-Actin↓, Tubulin↓	Cardiovascular function, organ morphology, DNA replication and repair	31
E2F6↑, Alpha tubulin↓, Hdac↓, HIST1H4C↑	Cancer, dermatological diseases, gastrointestinal disease	30
MMP15↓, IGF2↓, Collagen↑↓, Tgfb	Cellular proliferation, tumour morphology, infection mechanism	28
Collagen↑↓, COL1A1↓, PLAU↓, PI3K complex↑↓	Connective tissue disorders, genetic disorder, dermatological diseases	28
F-Actin↑↓, Pkc(s), Filamin, SNAP25↓	Cellular movement, nervous system function, neurological disease	27
CDK8↑, Histone H3↓, Mediator↑	Gene expression, amino acid metabolism, post-translational modification	27
TNFSF10↑, Jnk, Ubiquitin, Ikb↓	Infection mechanism, cell death, cellular development	25
ASB		
SRC↑, SNAP25↓	Cellular assembly/organisation, cellular maintenance, molecular transport	39
PRKACB↓, hCG complex↓	Cell signalling, molecular transport, nucleic acid metabolism	37
IGF1R↓, FGFR1/2↓	Cell death, cellular maintenance, cellular development	35
SPI1↑, Vegf, MHC Class II ↑	Inflammatory response, cellular assembly/organisation, cellular maintenance	32
TREM1 ↑, HDAC11 ↓	Cell-to-cell signalling, haematological system development, inflammatory response	30
NFκB complex	Cell-to-cell signalling, haematological system development, haematopoiesis	29
Akt, NCOR1 ↑	Drug metabolism, small-molecule biochemistry, gene expression	29
Creb, PCNA ↓, MMP2 ↓, FN1 ↓	Cellular movement, tumour morphology, cellular development	29
Erk, Tgfb, SMAD6/7 ↓	Cellular development, cellular proliferation, connective tissue development	27
SNCA, Caspase	Cell death, post-translational modification, protein folding	26

*Direction of arrow indicates over- or under-expression. Bold and lowercase letters indicate genes and complexes, respectively; †Genes or complexes with no arrow represent signalling hubs that were not differentially expressed; ‡Arrows (↑↓) represent multiple genes within a complex experiencing over- and under-expression, respectively.

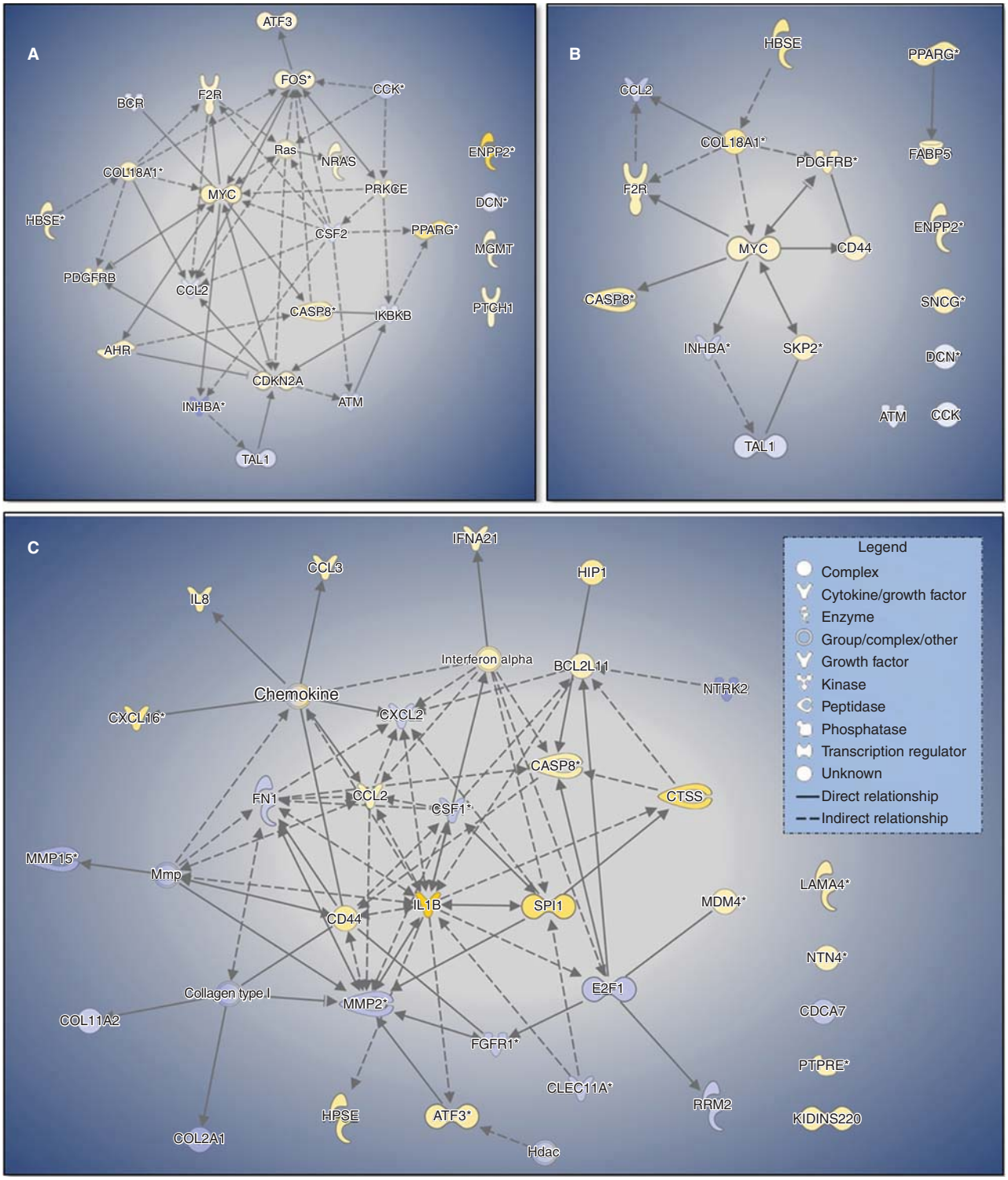

Figure 6. Cancer-promoting GSNs in A) D-SWCNT, B) D-MWCNT and C) ASB neoplastic-like transformed SAECs. DISP cell gene expression served as a comparative control. DEGs were first filtered for cancer-related activity. Next, genes that promoted cancer (over-expressed/promoted cancer and under-expressed/inhibited cancer) were included in the pathway. Genes were mapped with known direct and indirect signalling associations using IPA. Yellow and blue indicate over- and under-expressed genes, respectively, while intensity indicates magnitude of fold change.

gene signalling hubs. D-UFCB, D-SWCNT, D-MWCNT and ASB cells possessed over-expressed levels of IL-1β compared to both SAL and DISP controls with ASB displaying the highest IL-1β expression. ASB cells over-expressed both IL-8 and SPI1 compared to DISP cells, while both D-SWCNT and D-MWCNT possessed basal low expression level (Figure 7E). In summary, protein expression analysis confirmed a majority of the microarray expression data and displayed several differences between CNT SAECs and ASB SAECs.

Discussion

Current and future CNT manufacture for use in many different industrial, medical and consumer products requires

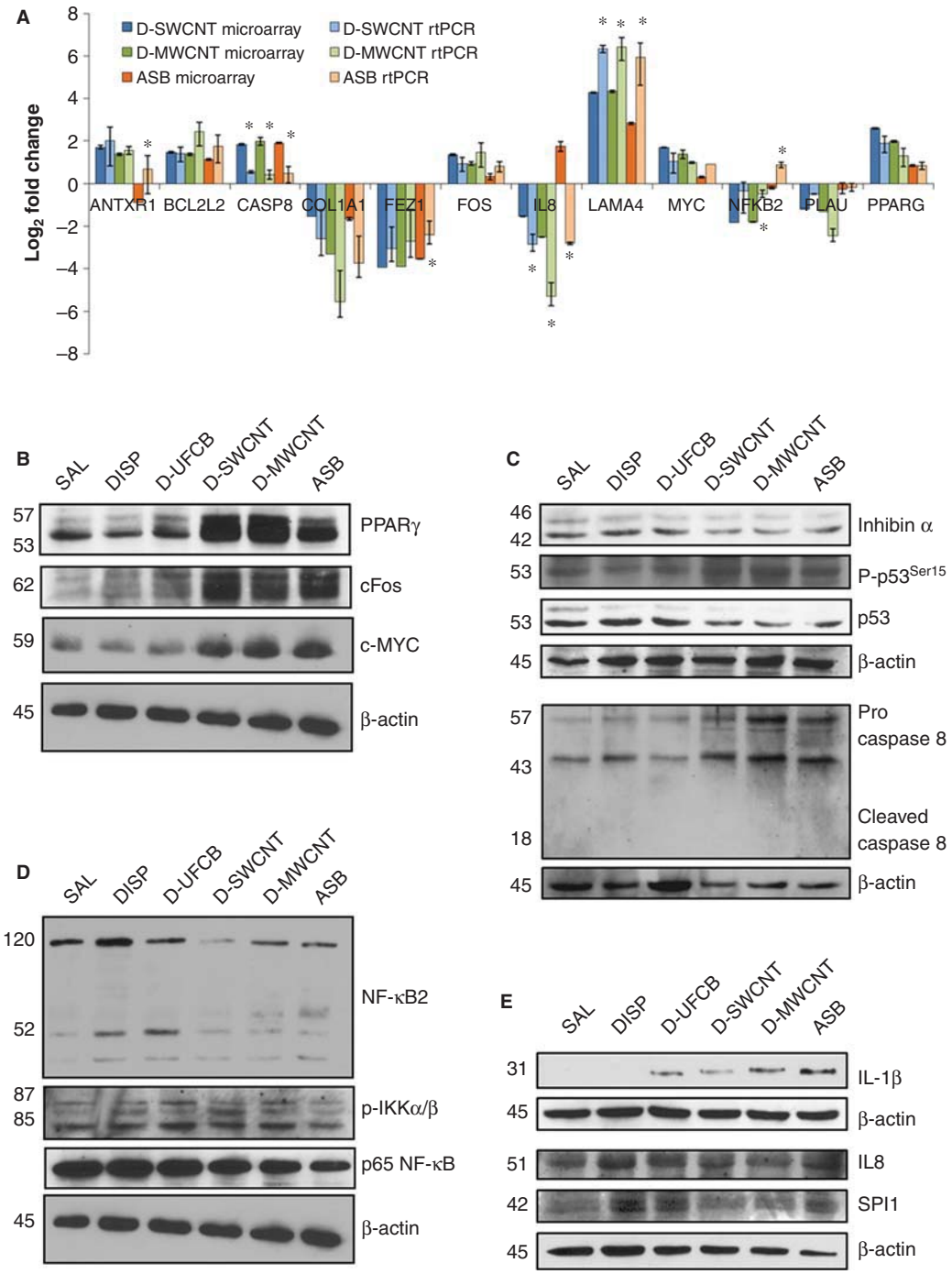

Figure 7. rtPCR validation of microarray and Western blot analysis of key proteins driving D-SWCNT and D-MWCNT vs. ASB cell neoplastic-like transformation signalling. A) Comparison of microarray to rtPCR expression of key transformation genes was performed. * indicates those rtPCR values that significantly differed from microarray gene expression. B) Over-expression of several proto-oncogenes associated with D-CNT and ASB cell signalling. C) Decreased tumour suppressor and increased caspase 8 expression in D-SWNCT, D-MWCNT and ASB cells. D) Decreased NF-κB expression in D-CNT cells. E) Over-expressed inflammasome-associated chemokines and a developmental regulator in ASB cells.

adequate research into benefits and health risks associated with these unique HAR nanomaterials. Given their physicochemical property and biological effect similarities to asbestos fibres, increased concern over a CNT-induced lung carcinogenesis has been identified. A preliminary inhalation exposure study recently reported that MWCNT promote lung carcinogenesis in a mouse initiation/promotion tumour model (Sargent et al. 2013). However, it is not known how different physicochemical properties of CNTs influence the potential for lung cancer development and whether these mechanisms are similar to asbestos. This study exposed human SAECs, a major target of inhaled CNT (Mercer et al. 2010), to a subchronic occupational relevant dose of dispersed SWCNT, MWCNT and crocidolite asbestos to compare particle property-dependent cancer-like behaviour and changes in toxicogenomic expression signatures. By identifying signalling mechanisms associated with neoplastic-like transformation, comparisons of physicochemical properties of

CNTs to a well-known carcinogenic HAR fibre can be made and lends urgently needed information for human health risk assessment.

Subchronic CNT exposure results in a distinct CNT-associated neoplastic-like transformation and proto-oncogene signalling

This study provides novel evidence supporting CNT-associated lung neoplastic-like transformation upon long-term *in vitro* exposure which differed from crocidolite asbestos. Subchronic (6-month) exposure of 0.02 μg/cm^2 dispersed SWCNT and MWCNT to SAECs resulted in increases in several cancer hallmarks including proliferation, morphological transformation, anchorage-independent growth, invasion/migration and angiogenesis compared to DISP control cells. Aggressive neoplastic-like behaviour correlated with several cancer-associated GSNs, pathways and key proto-oncogenes associated with cell proliferation, cell movement, cell death and lipid metabolism which largely differed from pro-inflammatory genome expression signature and protein expression in ASB SAECs. The moderate inflammation signature in SAL control cells (NF-κB and *VEGF*) compared to DISP cells likely stemmed from long-term passage and the absence of lung surfactant, a known inflammation suppressor (Wright et al. 2004). Previously, both SWCNT and MWCNT particles used in this study were shown to cause centrosome fragmentation, mitotic spindle disruption and aneuploidy in human small airway and bronchial epithelial cells during acute exposures (Sargent et al. 2009; Sargent et al. 2012) which are typically observed in cancer cells. Furthermore, these same CNTs were found to induce K-ras mutations following inhalation exposure in mice (Shvedova et al. 2008). Collectively, these results satisfy three out of the four major criteria for neoplastic transformation (OECD 2007; Creton et al. 2012) minus *in vivo* tumourigenesis after injection. These xenograft studies are currently underway at NIOSH.

Increased TF and altered morphology of both D-CNT cells vs. ASB cells provided the first evidence of a distinct CNT transformation effect. Morphological transformation evidenced by small Type III foci in both D-SWCNT and D-MWCNT cells correlated with transformation frequencies of Balb/3T3 cells exposed to functionalised MWCNT for 72 h (Ponti et al. 2012). Gross morphological assessment revealed CNT exposure-associated increase in the number of SAECs possessing multiple intracellular vesicles surrounding the nucleus. Their close association to the nucleus, Golgi apparatus and lysosomes suggests that these bodies are potentially associated with endocytotic uptake response to nanomaterial exposure, general xenobiotic exposure (Al-Jamal et al. 2011) or associated with enhanced synthesis/trafficking of intracellular material (i.e. lipid metabolism). Further evaluation of the potential role of this unique morphological characteristic is currently underway in our laboratory.

Several recent reviews on ENM toxicology have called for use of whole-genome/proteome expression assessments to help identify potential health risks associated with ENM exposure. Phenotypic anchoring of organismal or tissue behaviour with whole-genome expression signature profiling can determine differences between xenobiotic exposures and identify novel mechanisms of action (Ganter & Giroux 2008). Here, employment of whole-genome expression signature profiling following subchronic *in vitro* CNT exposure revealed novel signalling networks with known neoplastic effects in D-CNT cells with some stark differences to ASB cell neoplastic-like transformation signalling. Prior studies with acute SWCNT- and MWCNT-exposed cells displayed DNA damage, activated MAPKs, AP-1, NF-κB and Akt, all of which recapitulate key molecular events involved in asbestos-induced mesothelioma (Sharma et al. 2007; Chou et al. 2008; Pacurari et al. 2008a; Pacurari et al. 2008b; Lindberg et al. 2009; Hirano et al. 2010; Ponti et al. 2012; Sargent et al. 2012). Acute studies directly comparing different CNT morphologies to asbestos report greater SWCNT cytotoxicity than MWCNT while MWCNTs exhibit similar fibrotic effects in fibroblasts (Tian et al. 2006; Mishra et al. 2012). In addition, increased inflammatory signalling, altered actin cytoskeleton and cell morphogenesis in bronchial epithelial cells are known (Kim et al. 2012). These studies suggest that initial, acute lung epithelial response is largely dominated by inflammatory and fibrosis signalling.

Here, subchronic CNT exposure resulted in alteration of proto-oncogenes both observed in asbestos-associated lung disease and unique to CNT-exposed cells. Over-expression of *MYC*, *PPARG*, *CASP8* and *COL18A1* as major hub genes in both D-CNT SAEC cancer GSNs suggests a proto-oncogene-dominated genotype compared to ASB SAEC's pro-inflammatory genotype centred on over-expressed *IL-1B*, *CCL2*, *SRC* and *SPI1*. Up-regulation of *c-Myc*, *fra1* and *bcat* in mesothelioma in rats following asbestos intraperitoneal injection (Sandhu et al. 2000) parallels over-expression of *MYC*, *FOS* and *BCAT1* in D-SWCNT cells and *MYC* in D-MWCNT cells in the present study. *MYC* over-expression potentially represents a common response to HAR particles or a generalised response to xenobiotics since its acute over-expression drives apoptosis and other cell stress responses. Its persistent over-expression, however, is a well-established cancer promotion signal (Varella-Garcia 2010).

Key genes identified in the D-CNT cell GSN analysis exhibited mRNA and protein expression correlating with known cancer function. Several top up- and down-regulated genes were associated with extracellular matrix, cell motility and morphology. *ANTXR1* and *LAMA4* over-expression potentially contributed to enhanced invasion ability in CNT and ASB SAECs (Huang et al. 2008; Cullen et al. 2009). Conversely, large down-regulation of *COL1A1*, a known lung fibrosis marker, and *PLAU* with over-expression of *COL18A1* and several basal collagens (collagens IV, V and VI; data not shown) suggests a shift towards basal ECM adhesion and potential motility enhancement. Over-expression of *COL18A1* and collagens IV, V and VI is associated with poor clinical outcome in NSCLC patients and promotes cancer cell survival (Iizasa et al. 2004). *INHBA* and *ATM*, two anti-proliferation tumour suppressors commonly mutated in lung cancer (Ding et al. 2008), were down-regulated in D-CNT SAECs. Over-expression of *BCL2L2*, *CASP8*, *FOS* and *MYC* suggests substantial changes to survival, cell stress and cell death signalling pathways in CNT-

exposed SAECs. Although *CASP8*, *FOS* and *MYC* are involved in cellular stress response with known cell death signalling roles, they also display several tumour promotion functions including mitochondria stimulation, cell proliferation, migration and transformation and exhibit increased expression in lung cancer (Heintz et al. 2010; Varella-Garcia 2010; Kamp et al. 2011; Kober et al. 2011).

Decreased p53 expression with enhanced phospho-p53 (Ser15) suggests that subchronic CNT and ASB exposure suppressed basal p53 expression. Down-regulation (e.g. *ATM*) and up-regulation (e.g. *POLK*, *MGMT*) of DNA repair genes with decreased basal p53 expression in D-SWCNT SAECs suggest an altered ability to respond to potential DNA damage. However, enhanced Ser15 phosphorylation suggests an active tumour suppressor function by allowing binding to p300 or binding directly to DNA damage sites (Shanaz et al. 2005). This contradicts our previous finding in SWCNT-exposed BEAS-2B cells showing decreased phosphorylation (Wang et al. 2011b) potentially due to a weakened p53 following BEAS-2B immortalisation.

CNT subchronic exposure increases lipid metabolism signalling and *PPARG* over-expression

Subchronic SWCNT and MWCNT exposure caused large alterations in lipid metabolism suggesting that CNTs may drastically alter many energy, proliferation and oxidative stress pathways that rely on fatty acids and sterols. Few studies have acknowledged the role that CNT exposure may have in affecting lipid peroxidation, lipidomic response and lipid metabolic pathways in cells (Shvedova et al. 2012). Lipid peroxidation is known to activate peroxidation detoxification pathways including the peroxisome proliferator-activated receptors (PPARs). PPARs regulate lipid metabolism, retinoic acid signalling and are implicated in either promoting or inhibiting carcinogenic signalling in lung cancer. *PPARG* expression is typically observed in adipocytes, possesses potent anti-inflammatory properties and is a known prognostic marker in lung cancer with it over-expression indicating a favourable prognosis (Szanto & Nagy 2008; Peters et al. 2012). Over-expression of *PPARG* in both D-SWNCT and D-MWCNT SAECs suggests a potential role that lipid signalling and metabolism may play in these cells. Down-regulated *NFKB2*, a key hub gene in several top-ranked D-SWCNT and D-MWCNT GSNs associated with lipid metabolism (Table IV), suggests a potential relationship between *PPARG*, *NFKB2* and an anti-inflammatory genome expression signature. In addition, PPAR family activation promotes expression of several genes (i.e. *HMGCR*) that contributes to cancer promotion via lipid and cholesterol synthesis (Peters et al. 2012). Future studies should evaluate both lipid metabolism and PPAR expression to evaluate the role that CNT-induced alterations to cellular lipid peroxidation levels, lipid metabolism and suppressed immune function have on pulmonary tissue.

Differences in physicochemical properties impact nanomaterial neoplastic-like effects

Knowledge-based mapping of cancer GSNs identified a pro-inflammatory dominated genome expression signature in ASB SAECs which was largely absent in both D-CNT SAECs. Pulmonary exposure to HAR fibres results in an acute inflammatory response and infiltration of polymorphonuclear leukocytes and macrophages. Due to their long length, frustrated phagocytosis and activation of the NLRP3 inflammasome ensue (Palomaki et al. 2011). Protein over-expression of *IL1B* and *CCL2* is typically observed in lung lavage fluid following asbestos and CNT *in vivo* exposures (Jacobsen et al. 2009; Shvedova et al. 2005; Shvedova et al. 2008). Prolonged release of pro-inflammatory mediators results in activation of NF-κB and its downstream targets. Present hypotheses for ASB-mediated carcinogenesis focus on activation of tumour promotion signalling pathways via ROS generation and chronic inflammation (Nymark et al. 2007; Kamp 2009; Heintz et al. 2010; Kamp et al. 2011). Toxicogenome expression analysis of acute *in vitro* asbestos-exposed lung epithelial and mesothelial cells identified altered or enhanced NF-κB regulation, thioredoxin, Bcl-2, integrin, collagen, p53, caspase 8, c-Myc and Nrf2 signalling, most of which are known to occur in asbestos-associated lung cancers (Nymark et al. 2007; Hevel et al. 2008). Here, our subchronic exposure study's findings largely support a pro-inflammation hypothesis for asbestos-induced neoplasm and supplies additional novel insight for several key GSNs associated with such response. Top-ranked ASB GSNs and canonical pathways with over-expression of several integrin signalling genes (*ITGB2, SRC, TREM1, PI3K*) with down-regulated clathrins suggested adaptation to active uptake of asbestos fibres via integrin signalling and activation of NF-κB inflammatory pathways (Kamp 2009). Cell proliferation, cancer and tissue morphology behaviour were associated with the ASB pro-cancer GSN, suggesting an up-regulated inflammation response (Dostert et al. 2008). *SPI1* over-expression, a known regulator of haematopoiesis and leukocyte differentiation, with its association with several inflammatory genes suggests that it contributed to ASB cell neoplastic-like behaviour and was recently identified as a potential squamous lung cancer marker (Bai & Hu 2012). To our knowledge, this is the first time *SPI1* has been implicated in an asbestos-induced neoplastic-like mechanism. Many of the major expression changes observed in D-CNT SAECs were also observed in ASB SAECs (e.g. over-expressed *CASP8, MAP3K1, CD44* and c-Myc protein), albeit to a lesser extent. In conclusion, GSN analysis of the ASB cell signature overwhelming supported a pro-inflammatory signalling associated with several cancer hallmarks while the D-CNT cell signature favoured a large decrease in the innate immune system and NF-κB.

Conversely, subchronic UFCB exposure resulted in a non-neoplastic phenotype characterised by slow proliferation, low soft agar colony formation and a genome expression signature consistent with enhanced cell death, reduced neoplasia and reduced attachment ability. Prolonged UFCB exposure results in alveolar deposition, interstitial penetration, pulmonary inflammation and epithelial cytotoxicity leading to lesions and fibrosis (IARC 2010). UFCB is listed as a Group 2B possible human carcinogen with no clear risk of human lung cancer development in the occupational setting; however, female murine inhalation

exposure studies found increased risk for lung cancer (Borm et al. 2004). Our *in vitro* study differs from previous human and murine bronchial epithelial cell *in vitro* studies. Following relatively high exposure doses, cells exhibited increased ROS production, proliferation, kinase activation, epithelial growth factor receptor activation and weak mutagenesis (Tamaoki et al. 2004; Jacobsen et al. 2007). Although these studies suggest toxicological effects typical of known carcinogens, their reported acute or subchronic exposure doses were 17.6–2000 times greater than those tested in the present study. UFCB-induced ROS production leading to DNA damage is more likely due to an indirect mechanism via the 'particle overload' phenomenon and low clearance rates in both *in vivo* murine and *in vitro* exposure assessments (Oberdorster 2002; IARC 2010). In this study, the subchronic, low-dose exposure regime potentially did not result in a UFCB 'particle overload' mechanism leading to a neoplastic-like phenotype.

Differences in exposed cell behaviour, toxicogenome signatures and signalling pathways are potentially due to several physicochemical differences among particle types. HAR, presence/absence of metal impurities, major components (carbon vs. silica), surface area, uptake ability and internal dosimetry possibly contributed to the observed differences among exposed cells. High doses of long, thin MWCNTs compared to short and tangled MWCNTs were shown to cause increased damage and increased risk for mesothelioma (Nagai et al. 2011). CNTs containing large or minute amounts of metal catalysts caused enhanced ROS, inflammation and cytotoxicity both *in vitro* and *in vivo* (Lam et al. 2004; Shvedova et al. 2009; Hirano et al. 2010; Azad et al. 2012; Shvedova et al. 2012). Recent studies evaluating ENM dosimetry have repeatedly shown that surface area is a contributing factor to observed lung inflammation, fibrosis and potential carcinogenesis (Borm et al. 2004; Duffin et al. 2007; Murray et al. 2012). Surface area-based 'particle overload' also may occur with CNTs since they possess low mass but high surface areas (Donaldson & Poland 2012). Here, dispersed SWCNTs possessed a 10–100-fold increase in surface area compared to all other dispersed particles, while MWCNTs possessed a 2.6-fold increase in surface area over asbestos fibres. A greater surface area for SWCNTs and MWCNTs potentially contributed to the enhanced cancer hallmark behaviour compared to other treatment groups. UFCB's low aspect ratio with comparable surface area to MWCNTs suggests that HAR is a compelling factor in CNT toxicity (Donaldson et al. 2010). Conversely, qualitative analysis of particle uptake showed that a high number of dispersed MWCNT were co-localised with SAEC compared to equal doses ($\mu g/cm^2$) of other particles, which suggests the need to evaluate how ENM internal dosimetry drives short- and long-term health effects. Regardless of physicochemical and uptake differences, both D-CNT cells exhibited the most similar toxicogenome signatures and pro-cancer signalling networks. This suggests that a long-term, occupational exposure to a carbon-based nanofibre with relatively high surface area results in a neoplastic-like transformation effect that is unique from UFCB or asbestos fibres.

Potential suppressed immune response pathways following subchronic SWCNT and MWCNT exposure

Both D-CNT SAECs exhibited decreased gene expression in complement proteins, *NFKB2* and several known inflammation cytokines. Recent *in vivo* and *in vitro* studies have reported alterations and/or reductions in immune response following CNT exposure, possibly due to changes in lung cell signalling to the spleen, impaired macrophage function or excessive activation of complement proteins (Shvedova et al. 2008; Herzog et al. 2009; Mitchell et al. 2009; Tkach et al. 2011; Anderson et al. 2012). MCP-1 *(CCL2)*, a pulmonary inflammatory marker, consistently exhibits over-expression in mouse lung lavage following acute CNT exposure; however, a previous *in vitro* study found MCP-1 under-expression following SWCNT exposure (Herzog et al. 2009). Its decreased gene expression in D-CNT SAECs, along with other known inflammatory cytokines, suggests that inflammatory-related markers may only be relevant within short time frames following exposure. This is not a surprise since several studies show that the inflammatory response to CNT exposure is transient *in vivo* (Shvedova et al. 2005; Shvedova et al. 2012; Porter et al. 2010). Increased p-IKKa/B expression resulting in targeting p65 NF-κB and *NFKB2* down-regulation suggests that continuous, low-dose CNT exposure results in reduced lung epithelial cell innate and adaptive immune responses, respectively, potentially contributing to enhanced susceptibility to infection (Tkach et al. 2011). At present, the mechanism(s) driving a suppressed innate and inflammatory response following CNT exposure are unknown. Based on *in vitro* and *in vivo* results, future studies should focus on CNT and nanomaterial ability to weaken pulmonary immune response resulting in increased susceptibility to other insults.

Comparison to other *in vitro* transformation and *in vivo* toxicogenomic studies

Few *in vitro* studies have assessed prolonged, continuous exposure to CNTs compared to other well-categorised particles for potential health risks. This study contradicts the study by Thurnherr et al. (2011) that reported no long-term effects or adaptive mechanisms in A549 cells following continuous MWCNT exposure for 6 months at the 0.16 $\mu g/cm^2$. A549 cells were found to experience no changes in proliferation, morphology, ROS levels or cell death at 3 and 6 months post-exposure. Lung cancer, such as human A549 adenocarcinoma cells, exhibits several enhanced cancer hallmarks including enhanced cell proliferation and ROS levels (Azad et al. 2008). As such, they do not represent a normal, non-tumourigenic human airway epithelial cell to assess neoplastic transformation, but do serve as an appropriate acute exposure model for inflammation and cytotoxicity for particulate and CNTs (Herzog et al. 2009). Any MWCNT-induced changes were potentially masked or undetectable in an A549 cell model due to an already present malignant phenotype. Our previous study (Wang et al. 2011b) displaying SWCNT-induced neoplastic transformation in a non-tumourigenic bronchial epithelial cell (BEAS-2B) model coincides with the present study showing that the same SWCNT particles promoted increases in several cancer hallmarks.

Several recent published studies have reported *in vivo* proteomic and genetic responses following CNT exposure. Comparison of C57BL/6 mouse whole-lung proteomic responses to UFCB vs. SWCNT vs. asbestos at 24 h following a repeated aspiration exposure over 3 weeks found that SWCNT exhibited a more potent but similar inflammatory response to equal mass of crocidolite asbestos (Teeguarden et al. 2011). Major protein expression changes in haematopoiesis, endocytosis, chemotaxis, immune response and leukocyte activation for both SWCNT and asbestos coincide with this study's ASB SAEC cell toxicogenome signature. Agreement between both *in vitro* and *in vivo* profiling studies at 6-month and 3-week exposure time points, respectively, matches the chronic lung inflammation paradigm for asbestos and other HAR fibre lung disease (Kamp 2009; Broaddus et al. 2011). Two other biomarker studies screened known human lung cancer markers in whole mouse lung at 7–56-d post-exposure to aspirated MWCNT (Pacurari et al. 2011; Guo et al. 2012). These authors reported differential expression in 11 and 38 cancer-related gene subsets, respectively, in MWCNT-exposed lung and were associated with signal transduction, cell proliferation, cell cycle and cancer. Preliminary comparison of this study's CNT pro-cancer signalling results to gene markers from these two studies correlate poorly. This is due to potential differences in *in vitro* monolayer vs. whole lung *in vivo* response, species tested, time/dose differences and data set approach (i.e. whole-genome expression vs. human lung cancer marker set). Regardless, network analysis of an 11-gene biomarker set at 56-day post-exposure (Pacurari et al. 2011) did identify *PPARG* as a key signalling gene hub associated with other cancer and immune response signalling centred on tumour necrosis factor, interferon β and Bcl-2. Two genes, neuregulin (*NRG1*) and sonic hedgehog receptor (*PTCH1*), did exhibit differential expression in both this and the two *in vivo* biomarker studies following CNT exposure suggesting the potential importance of lung development signalling following CNT exposure. A more detailed *in vitro* to *in vivo* comparison is currently underway in a follow-up study using the reported D-SWNCT and D-MWCNT cell expression signatures to identify potential gene markers for use in CNT exposure risk assessment.

Although our chronic *in vitro* model successfully identified known carcinogenic gene signalling in ASB SAECs and distinct CNT neoplastic-like mechanisms, care must be taken in interpretation and applicability of these results. SAEC-hTERT cells were chosen based on their wild-type p53 status, known CNT interaction *in vivo* and non-tumourigenic status; however, they do exhibit drops in p16 expression after continuous long-term passage (Piao et al. 2005). These immortalised cell models, however, may represent the *in vivo* human lung epithelial cell condition since many lung cancers exhibit mutations in p53 and p16 (Ding et al. 2008). In addition, *in vivo* studies have shown that cell-to-cell signalling between epithelial, fibroblast and leukocyte cells following *in vivo* asbestos and CNT-exposure is largely inflammatory in nature (Shvedova et al. 2005; Porter et al. 2010; Matsuzaki et al. 2012). The absence of cells capable of releasing pro-inflammatory or other cell damage cytokines/chemokines (i.e. macrophages) in our system must be taken into account when considering the large down-regulation of inflammation-associated genes in D-SWCNT and D-MWCNT. Nevertheless, subchronic *in vitro* exposure models provide a rapid assessment tool to compare a multitude of different xenobiotics in a controlled manner and can assist in identifying mechanisms promoting disease.

Conclusion

Subchronic exposure of dispersed SWNCTs and MWCNTs to SAECs at doses relevant to those used in occupational exposure animal models resulted in a more aggressive, neoplastic-like phenotype than crocidolite asbestos, evidenced by increased levels in several cancer hallmarks: morphological transformation, proliferation, anchorage-independent growth, invasion, migration and angiogenesis. Furthermore, whole-genome expression profiling suggested that CNT-exposed cells possessed a distinct toxicogenomic signature compared to ASB cells, and that altered disease, cell, molecular and signalling pathway functions were consistent with known cancer cell signalling. CNT GSNs centred on increased expression of known lung cancer proto-oncogenes *MYC* and *PPARG* and decreased expression of known tumour suppressors (e.g. p53). Conversely, ASB cells exhibited pro-inflammatory signalling promoting established asbestos carcinogenesis pathways and mechanisms. Lastly, subchronic exposure to both D-SWCNT and D-MWCNT resulted in decreased NF-κB inflammatory signalling and complement protein expression that could potentially be linked to altered lipid metabolism and *PPARG* over-expression. This study's findings suggest that long-term CNT exposure to deep lung airway epithelial cells represents higher potential for carcinogenic risk than an equal dose of crocidolite asbestos, induces a CNT neoplastic-like transformation mechanism independent of known asbestos mechanisms, and possibly increases risk for lung infection due to innate immune system suppression. Follow-up studies using this data set will further identify CNT-associated signalling mechanisms promoting lung cancer cell-like signalling. Further implementation of chronic *in vitro* exposure model phenotype assessment coupled with toxicogenome expression profiling can identify key mechanistic differences and novel long-term health risks for different types of nanofibres and nanomaterials.

Acknowledgements

The authors appreciate Diane Schwegler-Berry and Sherri Friend for their technical assistance with image analyses. Many thanks to Jamie Barr for assistance with angiogenesis experiments and analysis.

Declaration of interest

This work was supported by the National Institute for Occupational Safety and Health and grants from the National Occupational Research Agenda (NORA FY09 LMW6), National Institutes of Health (R01-HL095579) and National Science Foundation (EPS-1003907). The findings and conclusions in this report are those of the authors and do not necessarily represent the views of the National Institute for Occupational Safety and Health.

References

Al-Jamal KT, Nerl H, Muller KH, Ali-Boucetta H, Li S, Haynes PD, et al. 2011. Cellular uptake mechanisms of functionalized multi-walled carbon nanotubes by 3D electron tomography imaging. Nanoscale 3:2627–2635.

Anderson AJ, Wibroe PP, Moghimi SM. 2012. Perspectives on carbon nanotube-mediated adverse immune effects. Adv Drug Deliv Rev; Epub. in press.

Aschberger K, Johnston HJ, Stone V, Aitken RJ, Hankin SM, Peters SA, et al. 2010. Review of carbon nanotubes toxicity and exposure—appraisal of human health risk assessment based on open literature. Crit Rev Toxicol 40. 759–790.

Azad N, Iyer AK, Wang L, Liu Y, Lu Y, Rojanasakul Y. 2012. Reactive oxygen species-mediated p38 MAPK regulates carbon nanotube-induced fibrogenic and angiogenic responses. Nanotox 7:157–168.

Azad N, Iyer AKV, Wang L, Lu Y, Medan D, Castranova V, et al. 2010. Nitric oxide-mediated bcl-2 stabilization potentiates malignant transformation of human lung epithelial cells. Am J Respir Mol Biol 42. 578:585.

Azad N, Rojanasakul Y, Vallyathan V. 2008. Inflammation and lung cancer: roles of reactive oxygen/nitrogen species. J Toxicol Environ Health B Crit Rev 11:1–15.

Bai J, Hu S. 2012. Transcriptome network analysis reveals potential candidate genes for squamous lung cancer. Int J Mol Med 29:95–101.

Borm PJ, Schins RP, Albrecht C. 2004. Inhaled particles and lung cancer, part B: paradigms and risk assessment. Int J Cancer 110:3–14.

Broaddus VC, Everitt JI, Black B, Kane AB. 2011. Non-neoplastic and neoplastic pleural endpoints following fiber exposure. J Toxicol Environ Health B 14:153–178.

Chou CC, Hsiao HY, Hong QS, Chen CH, Peng YW, Chen HW, et al. 2008. Single-walled carbon nanotubes can induce pulmonary injury in mouse model. Nano Lett 8:437–445.

Creton S, Aardema MJ, Carmichael PL, Harvey JS, Martin FL, Newbold RF, et al. 2012. Cell transformation assays for prediction of carcinogenic potential: state of the science and future research needs. Mutagenesis 27:93–101.

Cullen M, Seaman S, Chaudhary A, Yang MY, Hilton MB, Logsdon D, et al. 2009. Host-derived tumor endothelial marker 8 promotes the growth of melanoma. Cancer Res 69:6021–6026.

Ding L, Getz G, Wheeler DA, Mardis ER, McLellan MD, Cibulskis K, et al. 2008. Somatic mutations affect key pathways in lung adenocarcinoma. Nature 455:1069–1075.

Donaldson K, Murphy FA, Duffin R, Poland CA. 2010. Asbestos, carbon nanotubes and the pleural mesothelium: a review of the hypothesis regarding the role on long fibre retention in the parietal pleura, inflammation and mesothelioma. Part Fibre Toxicol 7:5.

Donaldson K, Poland CA. 2012. Inhaled nanoparticles and lung cancer – what we can learn from conventional particle toxicology. Swiss Med Wkly 142:w13547.

Dostert C, Petrilli V, Van Bruggen R, Steele C, Mossman BT, Tschopp J. 2008. Innate immune activation through Nalp3 inflammasome sensing of asbestos and silica. Science 320:674.

Duffin R, Tran L, Brown D, Stone V, Donaldson K. 2007. Proinflammogenic effects of low-toxicity and metal nanoparticles in vivo and in vitro: highlighting the role of particle surface area and surface reactivity. Inhal Toxicol 19:849–856.

Ganter B, Giroux CN. 2008. Emerging applications of network and pathway analyses in drug discovery and development. Curr Opin Drug Discov Dev 11:86–94.

Guo NL, Wan YW, Denvir J, Porter DW, Pacurari M, Wolfarth MG, et al. 2012. Multiwalled carbon nanotube-induced gene signatures in the mouse lung: potential predictive value for human lung cancer risk and prognosis. J Toxicol Environ Health A 75:1129–1153.

Hanahan D, Weinberg RA. 2011. Hallmarks of cancer: the next generation. Cell 144:646–674.

Heintz NH, Janssen-Heininger YM, Mossman BT. 2010. Asbestos, lung cancers, and mesotheliomas: from molecular approaches to targeting tumor survival pathways. Am J Respir Cell Mol Biol 42:133–139.

Herzog E, Byrne HJ, Casey A, Davoren M, Lenz AG, Maier KL, et al. 2009. SWCNT suppresses inflammatory mediator responses in human lung epithelium in vitro. Toxicol Appl Pharmacol 234:378–390.

Hevel JM, Olson-Buelow LC, Ganesan B, Stevens JR, Hardman JP, Aust AE, et al. 2008. Novel functional view of the crocidolite asbestos-treated A549 human lung epithelial transcriptome reveals an intricate network of pathways with opposing functions. BMC Genomics 9:376.

Hirano S, Fujitani Y, Furuyama A, Kanno S. 2010. Uptake and cytotoxic effects of multi-walled carbon nanotubes in human bronchial epithelial cells. Toxicol Appl Pharm 249:8–15.

Huang X, Ji G, Wu Y, Wan B, Yu L. 2008. LAMA4, highly expressed in human hepatocellular carcinoma from Chinese patients, is a novel marker of tumor invasion and metastasis. J Cancer Res Clin Oncol 134:705–714.

Hussain MA, Kabir MA, Sood AK. 2009. On the cytotoxicity of carbon nanotubes. Curr Sci 96:664–673.

Iizasa T, Chang H, Suzuki M, Otsuji M, Yokoi S, Chiyo M, et al. 2004. Overexpression of collagen XVIII is associated with poor outcome and elevated levels of circulating serum endostatin in non-small cell lung cancer. Clin Cancer Res 10:5361–5366.

International Agency for Research on Cancer (IARC). 2010. Carbon Black. IARC Monographs 93:1–149.

Jacobsen NR, Moller P, Jensen KA, Vogel U, Ladefoged O, Loft S, et al. 2009. Lung inflammation and genotoxicity following pulmonary exposure to nanoparticles in ApoE-/- mice. Part Fibre Toxicol 6:2.

Jacobsen NR, Saber AT, White P, Moller P, Pojana G, Vogel U, et al. 2007. Increased mutant frequency by carbon black, but not quartz, in the lacZ and cII transgenes of muta mouse lung epithelial cells. Environ Mol Mutagen 48:451–461.

Kamp DW, Shacter E, Weitzman SA. 2011. Chronic inflammation and cancer: the role of the mitochondria. Oncology 25:400–413.

Kamp DW. 2009. Asbestos-induced lung diseases: an update. Transl Res 153:143–152.

Kim JS, Song KS, Lee JK, Choi YC, Bang IS, Kang CS, et al. 2012. Toxicogenomic comparison of multi-wall carbon nanotubes (MWCNTs) and asbestos. Arch Toxicol 86:553–562.

Kober AMM, Legewie S, Pforr C, Fricker N, Eils R, Krammer PH, et al. 2011. Caspase-8 activity has an essential role in CD95/Fas-mediated MAPK activation. Cell Death Dis 2:e212.

Lam CW, James JT, McCluskey R, Hunter RL. 2004. Pulmonary toxicity of single-walled carbon nanotubes in mice 7 and 90 days after intratracheal instillation. Toxicol Sci 77:126–134.

Lindberg HK, Falck GC, Suhonen S, Vippola M, Vahala E, Catalan J, et al. 2009. Genotoxicity of nanomaterials: DNA damage and micronuclei induced by carbon nanotubes and graphite nanofibers in human bronchial epithelial cells in vitro. Toxicol Lett 186:166–173.

Matsuzaki H, Maeda M, Lee S, Nishimura Y, Kumagi-Takei N, Hayashi H, et al. 2012. Asbestos-induced cellular and molecular alteration of immunocompetent cells and their relationship with chronic inflammation and carcinogenesis. J Biomed Biotechnol 2012:492608.

Mercer RR, Hubbs AF, Scabilloni JF, Wang L, Battelli LA, Castranova V, et al. 2012. Pulmonary fibrotic response from inhaled multwalled carbon nanotube exposure in mice. Toxicologist 126: A1806–A1388.

Mercer RR, Hubbs AF, Scabilloni JF, Wang L, Battelli LA, Friend S, et al. 2011. Pulmonary fibrotic response to aspiration of multi-walled carbon nanotubes. Part Fibre Toxicol 8:21.

Mercer RR, Hubbs AF, Scabilloni JF, Wang L, Battelli LA, Schwegler-Berry D, et al. 2010. Distribution and persistence of pleural penetrations by multi-walled carbon nanotubes. Part Fibre Toxicol 7:28.

Mercer RR, Scabilloni JF, Wang L, Kisin E, Murray AR, Schwegler-Berry D, et al. 2008. Alteration of deposition pattern and pulmonary response as a result of improved dispersion of aspirated single-walled carbon nanotubes in a mouse model. Am J Physiol Lung Cell Mol Physiol 294:L87–L97.

Mishra A, Rojanasakul Y, Chen BT, Castranova V, Mercer RR, Wang L. 2012. Assessment of pulmonary fibrogenic potential of multiwalled carbon nanotubes in human lung cells. J Nanomater 2012:930931.

Mitchell LA, Lauer FT, Burchiel SW, McDonald JD. 2009. Mechanisms for how inhaled multiwalled carbon nanotubes suppress systemic immune function in mice. Nat Nanotechnol 4:451–456.

Msiska Z, Pacurari M, Mishra A, Leonard SS, Castranova V, Vallyathan V. 2010. DNA double-strand breaks by asbestos, silica and titanium dioxide: possible biomarker of carcinogenic potential? Am J Respir Cell Mol Biol 43:210–219.

Muller J, Huaux F, Moreau N, Misson P, Heilier JF, Delos M, et al. 2005. Respiratory toxicity of multi-wall carbon nanotubes. Toxicol Appl Pharmacol 207:221–231.

Murphy FA, Poland CA, Duffin R, Al-Jamal KT, Ali-Boucetta H, Nunes A, et al. 2011. Length-dependent retention of carbon nanotubes in the pleural space of mice initiates sustained inflammation and progressive fibrosis on the parietal pleura. Am J Pathol 178:2587–2600.

Murray AR, Kisin ER, Tkach AV, Yanamala N, Mercer RR, Young SH, et al. 2012. Factoring-in agglomeration of carbon

nanotubes and nanofibers for better prediction of their toxicity versus asbestos. Part Fibre Toxicol 9:10.
Nagai H, Okazaki Y, Chew SH, Misawa N, Yamashita Y, Akatsuka S, et al. 2011. Diameter and rigidity of multiwalled carbon nanotubes are critical factors in mesothelial injury and carcinogenesis. Proc Nat Acad Sci 108:e1330–e1338.
Nymark P, Lindholm PM, Korpela MV, Lahti L, Ruosaari S, Kaski S, et al. 2007. Gene expression profiles in asbestos-exposed epithelial and mesothelial lung cell lines. BMC Genomics 8:62.
Oberdorster G. 2002. Toxicokinetics and effects of fibrous and nonfibrous particles. Inhal Toxicol 14:29–56.
OECD. 2007. Detailed review on cell transformation assays for detection of chemical carcinogens. OECD Environment, Health and Safety, Series on Testing and Assessment, 31.
Pacurari M, Qian Y, Porter DW, Wolfarth M, Wan Y, Luo D, et al. 2011. Multi-walled carbon nanotube-induced gene expression in the mouse lung: association with lung pathology. Toxicol Appl Pharmacol 255:18–31.
Pacurari M, Yin XJ, Ding M, Leonard SS, Schwegler-Berry D, Ducatman BS, et al. 2008a. Oxidative and molecular interactions of multi-wall carbon nanotubes (MWCNT) in normal and malignant human mesothelial cells. Informa Healthcare 2:155–170.
Pacurari M, Yin XJ, Zhao J, Ding M, Leonard SS, Schwegler-Berry D, et al. 2008b. Raw single-wall carbon nanotubes induce oxidative stress and activate MAPKs, AP-1, NF-kappaB, and Akt in normal and malignant human mesothelial cells. Environ Health Perspect 116:1211–1217.
Palomaki J, Valimaki E, Sund J, Vippola M, Clausen PA, Jensen KA, et al. 2011. Long, needle-like carbon nanotubes and asbestos activate the NLRP3 inflammasome through a similar mechanism. ACS Nano 5:6861–6870.
Peters JM, Shah YM, Gonzalez FJ. 2012. The role of peroxisome proliferator-activated receptors in carcinogenesis and chemoprevention. Nat Cancer Rev 12:181–195.
Piao CQ, Li L, Zhao YL, Balajee AS, Masao Suzuki M, Hei TK. 2005. Immortalizaiton of human small airway epithelial cells by ectopic expression of telomerase. Carcinog 26:725–731.
Poland CA, Duffin R, Kinloch I, Maynard A, Wallace WA, Seaton A, et al. 2008. Carbon nanotubes introduced into the abdominal cavity of mice show asbestos-like pathogenicity in a pilot study. Nat Nanotechnol 3:423–428.
Ponti J, Broggi F, Mariani V, De Marzi L, Colognato R, Marmorato P, et al. 2012. Morphological transformation induced by multiwall carbon nanotubes on Balb/3T3 cell model as an in vitro end point of carcinogenic potential. Nanotox 7:221–233.
Porter DW, Hubbs AF, Mercer RR, Wu N, Wolfarth MG, Sriram K, et al. 2010. Mouse pulmonary dose- and time course-responses induced by exposure to multi-walled carbon nanotubes. Toxicol 269:136–147.
Roco MC. 2005. Environmentally responsible development of nanotechnology. Environ Sci Technol 39:106A–112A.
Saeed AI, Bhagabati NK, Braisted JC, Liang W, Sharov V, Howe EA, et al. 2006. TM4 microarray software suite. Methods Enzymol 411:134–193.
Sandhu D, Dehnen W, Roller M, Abel J, Unfried K. 2000. mRNA expression patterns in different stages of asbestos-induced carcinogenesis in rats. Carcinog 21:1023–1029.
Sargent LM, Hubbs AF, Young SH, Kashon ML, Dinu CZ, Salisbury JL, et al. 2012. Single-walled carbon nanotube-induced mitotic disruption. Mutat Res 745:28–37.
Sargent LM, Porter DW, Lowry DT, Battelli L, Siegrist K, Kashon ML, et al. 2013. Multiwalled carbon nanotube-induced lung tumors. Toxicologist 130:457.
Sargent LM, Shvedova AA, Hubbs AF, Salisbury JL, Benkovic SA, Kashon ML, et al. 2009. Induction of aneuploidy by single-walled carbon nanotubes. Environ Mol Mutag 50:708–717.
Sasaki K, Bohnenberger S, Hayashi K, Kunkelmann T, Muramatsu D, Poth A, et al. 2012. Photo catalogue for the classification of foci in the BALB/c 3T3 cell transformation assay. Mut Res 744:42–53.
Shanaz TAR, Dellaire G, Cuddihy A, Jalali F, Vaid M, Coackley C, et al. 2005. Evidence for the direct binding of phosphorylated p53 to sites of DNA breaks in vivo. Cancer Res 65:10–10821.
Sharma CS, Sarkar S, Periyakaruppan A, Barr J, Wise K, Thomas R, et al. 2007. Single-walled carbon nanotubes induces oxidative stress in rat lung epithelial cells. J Nanosci Nanotechnol 7:2466–2472.
Shvedova AA, Fabisiak JP, Kisin ER, Murray AR, Roberts JR, Tyurina YY, et al. 2008. Sequential exposure to carbon nanotubes and bacteria enhances pulmonary inflammation and infectivity. Am J Respir Cell Mol Biol 38:579–590.
Shvedova AA, Kisin ER, Mercer RR, Murray AR, Johnson VJ, Potapovich AI, et al. 2005. Unusual inflammatory and fibrogenic pulmonary responses to single-walled carbon nanotubes in mice. Am J Physiol Lung Cell Mol Physiol 289:L698–L708.
Shvedova AA, Kisin ER, Porter D, Schulte P, Kagan VE, Fadeel B, et al. 2009. Mechanisms of pulmonary toxicity and medical applications of carbon nanotubes: Two faces of Janus? Pharmacol Ther 121:192–204.
Shvedova AA, Pietroiusti A, Fadeel B, Kagan VE. 2012. Mechanisms of carbon nanotube-induced toxicity: focus on oxidative stress. Toxico. Appl. Pharm 261:121–133.
Stone KC, Mercer RR, Gehr P, Stockstill B, Crapo JD. 1992. Allometric relationships of cell numbers and size in the mammalian lung. Am J Respir Cell Mol Biol 6:235–243.
Stueckle TA, Lu Y, Davis ME, Wang L, Jiang BH, Holaskova I, et al. 2012. Chronic occupational exposure to arsenic trioxide induces carcinogenic gene signaling networks and neoplastic transformation in human lung epithelial cells. Toxicol Appl Pharm 261:204–216.
Szanto A, Nagy L. 2008. The many faces of PPARgamma: anti-inflammatory by any means? Immunobiol 213:79–82.
Takagi A, Hirose A, Nishimura T, Fukumori N, Ogata A, Ohashi N, et al. 2008. Induction of mesothelioma in p53+/- mouse by intraperitoneal application of multi-walled carbon nanotube. J Toxicol Sci 33:105–116.
Tamaoki J, Isono K, Takeyama K, Tagaya E, Nakata J, Nagai A. 2004. Ultrafine carbon black particles stimulate proliferation of human airway epithelium via EGF receptor-mediated signaling pathway. Am J Physiol Lung Cell Mol Physiol 287:L1127–L1133.
Teeguarden JG, Webb-Robertson BJ, Waters KM, Murray AR, Kisin ER, Varnum SM, et al. 2011. Comparative proteomics and pulmonary toxicity of instilled single-walled carbon nanotubes, crocidolite asbestos, and ultrafine carbon black in mice. Toxicol Sci 120:123–135.
Thurnherr T, Brandenberger C, Fischer K, Diener L, Manser P, Maeder-Althaus X, et al. 2011. A comparison of acute and long-term effects of industrial multiwalled carbon nanotubes on human lung and immune cells in vitro. Toxicol Lett 200:176–186.
Tian F, Cui D, Schwarz H, Estrada GG, Kobayashi H. 2006. Cytotoxicity of single-wall carbon nanotubes on human fibroblasts. Toxicol In Vitro 20:1202–1212.
Tkach AV, Shurin GV, Shurin MR, Kisin ER, Murray AR, Young SH, et al. 2011. Direct effects of carbon nanotubes on dendritic cells induce immune suppression upon pulmonary exposure. ACS Nano 5:5755–5762.
Varella-Garcia M. 2010. Chromosomal and genomic changes in lung cancer. Cell Adh Migr 4:100–106.
Vanparys P, Corvi R, Aardema M, Gribaldo L, Hayashi M, Hoffman S, Schechtman L. 2011. ECVAM prevalidation of three cell transformation assays. ALTEX 28:56–59.
Wang L, Castranova V, Mishra A, Chen B, Mercer RR, Schwegler-Berry D, et al. 2010. Dispersion of single-walled carbon nanotubes by a natural lung surfactant for pulmonary in vitro and in vivo toxicity studies. Part Fibre Toxicol 7:31.
Wang L, Luanpitpong S, Castranova V, Tse W, Lu Y, Pongrakhananon V, et al. 2011b. Carbon nanotubes induce malignant transformation and tumorigenesis of human lung epithelial cells. Nano Lett 11:2796–2803.
Wang X, Xia T, Ntim SA, Ji Z, Lin S, Meng H, et al. 2011a. Dispersal state of multiwalled carbon nanotubes elicits profibrogenic cellular responses that correlate with fibrogenesis biomarkers and fibrosis in the murine lung. ACS Nano 5:9772–9787.
Wright JR. 2004. Host defense functions of pulmonary surfactant. Biol Neonate 85:326–332.
Yin Q, Brody AR, Sullivan DE. 2007. Laser capture microdissection reveals dose-response of gene expression in situ consequent to asbestos exposure. Int J Exp Pathol 88:514–425.

Supplementary material available online

Supplementary Tables S1 and S2.
Supplementary Figures S1–S6.